Bioorganic Chemistry 99 (2020) 103629

Contents lists available at ScienceDirect

Bioorganic Chemistry

journal homepage: www.elsevier.com/locate/bioorg

Novel diindoloazepinone derivatives as DNA minor groove binding agents with selective topoisomerase I inhibition: Design, synthesis, biological evaluation and docking studies

Manasa Kadagathur[a], G. Parimala Devi[b], Preeti Grewal[c], Dilep Kumar Sigalapalli[a], Priyanka N. Makhal[a], Uttam Chand Banerjee[c,*], Nagendra Babu Bathini[b,*], Neelima D. Tangellamudi[a,*]

[a] Department of Medicinal Chemistry, National Institute of Pharmaceutical Education and Research (NIPER), Hyderabad 500037, India
[b] Department of Fluoro-Agrochemicals, CSIR-Indian Institute of Chemical Technology, Hyderabad 500007, India
[c] Department of Pharmaceutical Technology (Biotechnology), National Institute of Pharmaceutical Education and Research (NIPER), SAS Nagar, Punjab 160062, India

ARTICLE INFO

Keywords:
Indoloazepinone
Diindoloazepinone
Anticancer activity
DNA minor groove binding
Selective topoisomerase I inhibitor
Molecular Docking

ABSTRACT

We present here-in the molecular design and chemical synthesis of a novel series of diindoloazepinone derivatives as DNA minor groove binding agents with selective topoisomerase I inhibition. The *in vitro* cytotoxicity of the synthesized compounds was evaluated against four human cancer cell lines including DU143, HEPG2, RKO and A549 in addition to non-cancerous immortalized human embryonic kidney cells (HEK-293). Compound **11** showed significant cytotoxicity against all the four human cancer cell lines with IC_{50} values ranging from 4.2 to 6.59 μM. **11** was also found to display 13-fold selective cytotoxicity towards A549 cancerous cells compared to the non-cancerous cell lines (HEK-293). The decatenation, DNA relaxation and intercalation assays revealed that the investigational compounds **10** and **11** act as highly selective inhibitors of Topo-I with DNA minor groove binding ability which was also supported by the results obtained from circular dichroism (CD), UV-visible spectroscopy and viscosity studies. Apoptosis induced by the lead **11** was observed using morphological observations, AO/EB and DAPI staining procedures. Further, dose-dependent increase in the depolarization of mitochondrial membrane was also observed through JC-1 staining. Annexin V-FITC/PI assay confirmed that **11** induced early apoptosis. Additionally, cell cycle analysis indicated that the cells were arrested at sub-G1 phase. Gratifyingly, *in silico* studies demonstrated promising interactions of **11** with the DNA and Topo I, thus supporting their potential DNA minor groove binding property with relatively selective Topo I inhibition compared to Topo II.

1. Introduction

One of the primary objectives of a medicinal chemist is the discovery of new, efficient and safer chemotherapeutic agents. In the recent past, interest has been particularly drawn to that group of agents that target the human DNA [1]. The major step in DNA replication is DNA relaxation (releasing entanglement), which is performed by DNA topoisomerases I and II [2–4]. Topoisomerase II (Topo II) introduces splits into the double-strand DNA segments and transports another DNA helix through the cut segments, thus, untangling the DNA duplexes. Topoisomerase I (Topo I) is another nuclear enzyme that mediates the relaxation of both positively and negatively supercoiled DNA *via* reversible DNA single-strand cleavage and religation which is essential for replication and transcription progression [2]. This fact makes them important targets for several chemotherapeutic agents. Topoisomerase I inhibitors prevent the religation step by stabilizing the transient topoisomerase I–DNA covalent complex.

The cellular processes in cancer cells are more susceptible to DNA-interactive drugs than their normal counterparts. Thus, DNA has been considered as potential target for the development of anticancer modalities [5]. The minor groove of double helical B-DNA is a site of non-covalent interactions that are highly specific to AT-rich sequence, thus making the binding of nonintercalators (termed as minor-groove binders, MGBs) to minor groove a novel chemotherapeutic approach. MGBs contain several fused aromatic rings arranged in a crescent shape rendering very similar dimensions as that of base pairs thereby

* Corresponding authors.
E-mail address: neelima@niperhyd.ac.in (N.D. Tangellamudi).

https://doi.org/10.1016/j.bioorg.2020.103629
Received 1 November 2019; Received in revised form 18 January 2020; Accepted 26 January 2020
Available online 28 January 2020

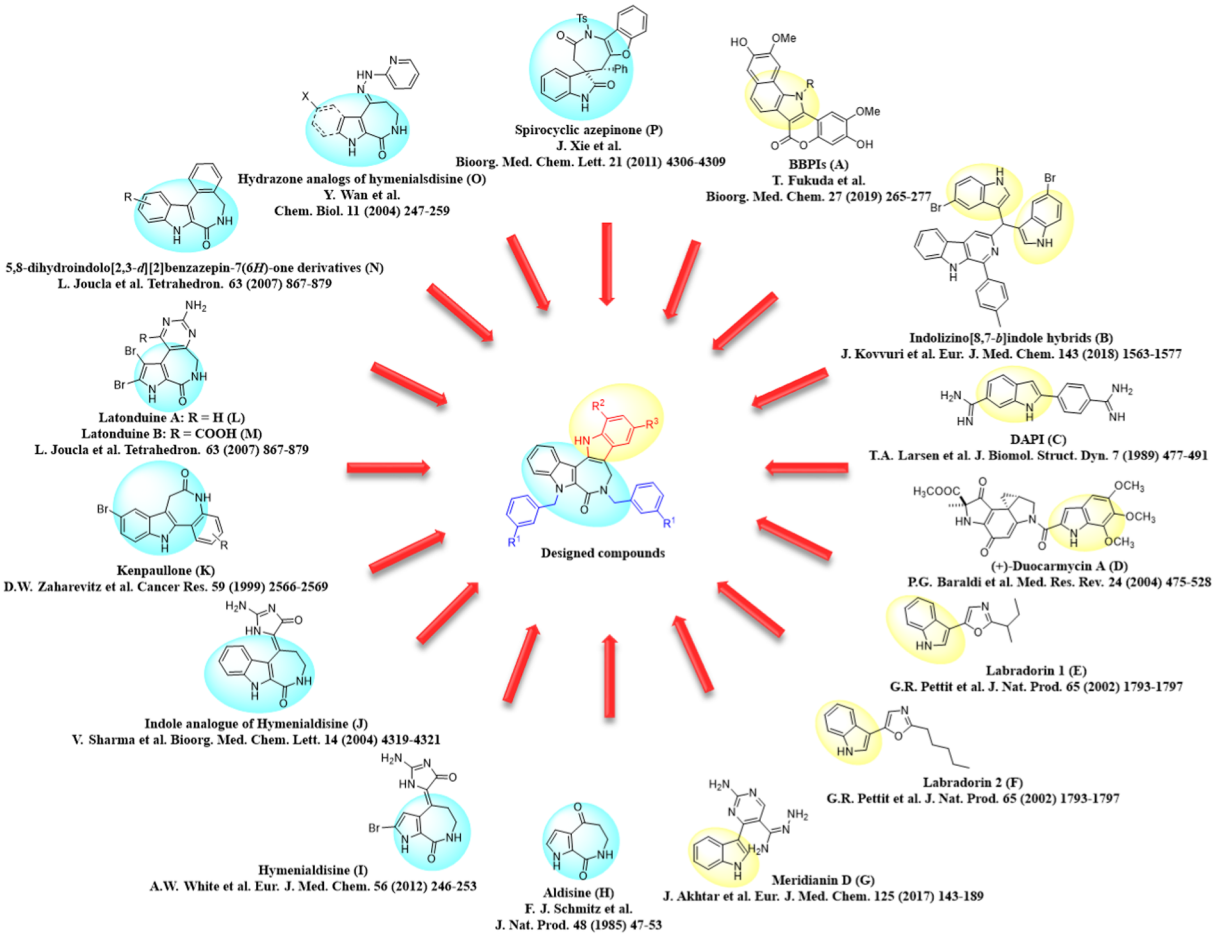

Fig. 1. Anticancer agents containing indole and heteroaromatic-fused azepinone moiety.

complementing the shape of the groove [6]. Moreover, MGBs also showcase hydrophobic interactions in addition to the common ionic contacts [7].

N-containing heterocyclic rings generally offer a polarized character which helps in increasing the stability of the molecule-receptor complex by establishing optimum interaction with the receptor and thus, produce anticancer effects [8]. In particular, the structural diversity of biologically active indoles [9] (A-G, Fig. 1) and seven-membered rings makes them important structural components in many pharmaceutical agents [8,10–15]

Azepines and azepinones have recently gained a considerable amount of attention and interest because of their continuing pharmacological significance. Many natural products and reported scaffolds with anticancer property were found to normally contain tetrahydroazepinone pharmacophore fused with a heterocycle, such as indole, pyrrole or benzofuran, as their main component (H–P, Fig. 1) [16–26].

Tailor-made design of the molecules by fusion of two or more heterocyclic rings in a single molecular frame renders better pharmacokinetic properties and improved molecular interactions between the drug and its cellular target. [8,27]. Syntheses of such hybrid molecules by amalgamation of two molecular entities are fascinating to work upon for developing modified scaffolds with unusual and greatly improved properties in the area of medical science [28]. In addition, the introduction of backbone rigidity and/or the conformational control of molecular scaffolds through cyclization [24] have been proven to have a beneficial effect on pharmacological efficiency. In view of the potential antiproliferative effect of indole and indole-fused azepinones, and recognizing the conformation control and enhanced synergistic effects that the ring fusion concepts offer, we were prompted to fuse indole and azepinone (aldisine) in a single heteroaromatic framework to afford conformationally constrained diheterocyclic azepinone analogues with potential antiproliferative effect. With this rationale, the designed analogues were synthesized and evaluated for their *in vitro* cytotoxicity, DNA binding and topoisomerase inhibition studies to obtain highly promising results.

2. Results and discussion

2.1. Chemistry

A library of diindoloazepinone analogues comprising 25 compounds were synthesized. The synthesis of the desired intermediate, indoloazepinone **5**, was achieved by the method outlined in Scheme 1, as per the reported method [29]. EDC·HCl along with DMAP was used for the coupling of indole-2-carboxylic acid **1** with β-alanine ethyl ester **2** to give the intermediate **3** in high yield of 90%. Basic hydrolysis yielded the cyclisation precursor **4**. Further, cyclodehydration was carried out in the presence of phosphorous pentoxide in methanesulfonic acid to give indoloazepinone **5** in 60% yield. *N*-alkylated indoloazepinones **7a-b** were prepared according to a reported protocol [26] by treating **5** with the respective benzylbromides **6a-b** in the presence of potassium carbonate as base, which was confirmed by the disappearance of indolic N–H peak in ^{1}H NMR at 12.47 ppm with amidic N–H seen at 8.90 ppm, whereas, *N,N*-dialkylated indoloazepinones **8a-b** were obtained from the reaction between indoloazepinone **5** and benzylbromides **6a-b** by the employment of a stronger base – sodium hydride. The *N,N*-dialkylation of indoloazepinone could be confirmed by the disappearance of

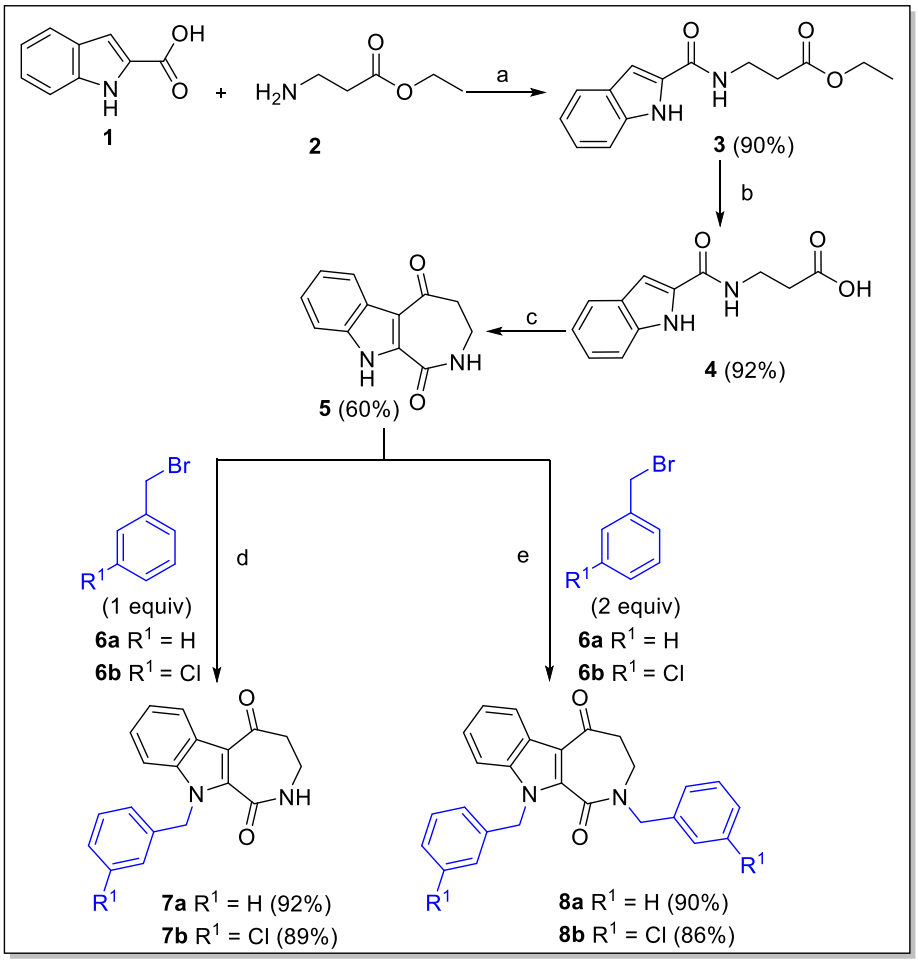

Scheme 1. Reagents and conditions: (a) EDCI·HCl (2 equiv), DMAP (2.2 equiv), DMF, rt, N_2, 20 h; (b) NaOH (3 equiv), EtOH, rt, 30 min; (c) P_2O_5 (1.2 equiv), $MeSO_3H$ (1 equiv), 85–110 °C, 2 h; (d) K_2CO_3 (3 equiv), DMF, 0 °C to reflux, 8 h; (e) NaH (2 equiv), DMF, 0 °C to rt, 12 h.

both indolic (12.47 ppm) and amidic N−H peaks (8.90 ppm) from ^{1}H NMR (experimental section).

Scheme 2 shows the preparation of diindoloazepinone carried out by Fischer indole synthesis [30]. Employing this well-known method, the analogues (**10–34**) were prepared by reacting the substituted and unsubstituted indoloazepinones with appropriate phenylhydrazines **9** in ethanol: glacial acetic acid (1:1). Cyclization and aromatization of the intermediate hydrazones with loss of ammonia, upon addition of concentrated HCl, provided the desired diindoloazepinone products.

2.2. Biological evaluation

2.2.1. Cytotoxic assays

The cytotoxicity of the synthesized library of compounds was evaluated *in vitro* against DU143, HEPG2, RKO, A549 and HEK-293 with doxorubicin as a positive control. As a screening assay, the cytotoxicity was expressed in terms of IC_{50} values (concentration of the drug causing 50% inhibition of the cell growth) by taking into account the upshots of the MTT tetrazolium reduction assay. Results shown in Table 1 indicate that the diindoloazepinone derivatives displayed good cytotoxicity with their IC_{50} values in the range of 4.2–89.6 μM.

Compounds **10–13**, **16, 18, 19, 24** and **26** showed good activity with their IC_{50} values < 10 μM for, at least, one of the cell lines tested, while the **11** exhibited high level of cytotoxicity against all the cell lines screened initially which encouraged us to choose **11** for further investigation of mechanistic studies. To determine if our newly synthesized compounds have differential cytotoxic effects on cancerous and noncancerous cells, the cytotoxicity of **10**, **11** and **13** was also evaluated on HEK-293 non-cancerous immortalized human embryonic kidney cells. We found that the tested compounds displayed 13-fold selectivity to A549 cancerous cell lines over HEK-293 non-cancerous cell lines.

Compound **10** containing unsubstituted indolic and amidic nitrogens, showed an IC_{50} of 8.9 μM on HEPG2 cell line and ≤15 μM on other tested cell lines. Methyl substitution at the C_4 position on the newly formed indole ring, yielded a more potent analogue **11** with a 4-fold and 2-fold increase in the activity as compared to the unsubstituted **10** in A549 and HEPG2 cell lines, respectively. Fluoro (**12**) and chloro (**13**) substitutions were acceptable modifications which showed nearly comparable activities as that of **11**. Compound **14** which flaunted a bromo substitution resulted in slightly diminished activities in all the tested cell lines. *N*-alkylated analogues with electron withdrawing groups (**18–20, 24** and **26**) on the newly formed indole ring gave better activities, whereas decreased potency was witnessed as an effect of electron donating groups as can be seen in **17, 21** and **23**. The importance of the free amidic N−H was emphasized by the negligible activity of the *N,N*-dialkylated analogues **28–31**, **33** and **34**. Nevertheless, compound **32** did preserve its cytotoxic activity with IC_{50} < 20 μM in all the tested cell lines. It is noteworthy to emphasize on the importance of fluoro-substitution on the newly formed indole ring (at R^3, as seen in **12**, **18**, **24** and **30**), which showed good activity in A549 cell line (ranging from 5.23 to 12.5 μM), irrespective of the substitution on nitrogen atoms. The structure activity relationship is summarized in Fig. 2.

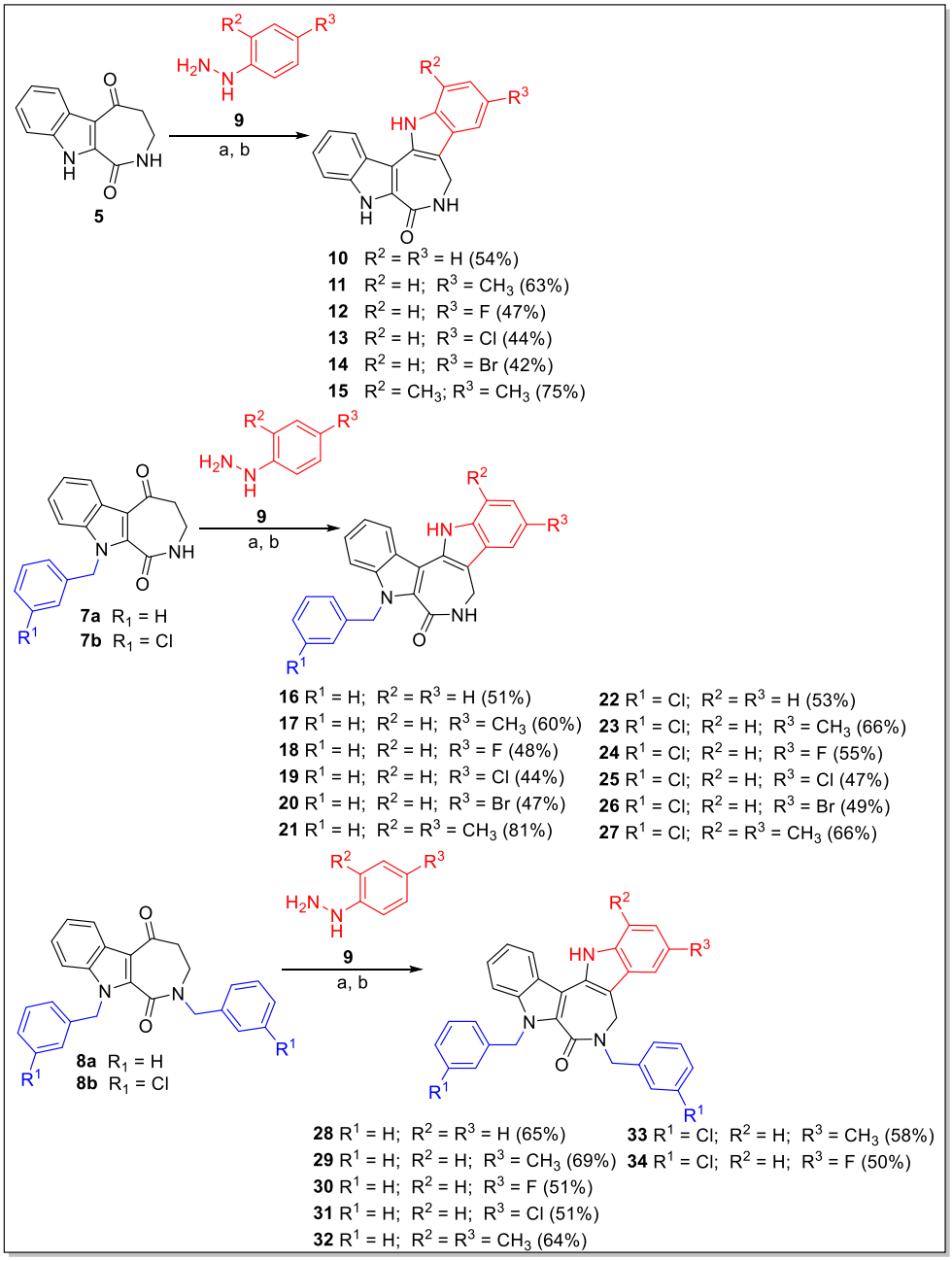

Scheme 2. Reagents and conditions: (a) CH_3COOH:EtOH (1:1), (b) HCl reflux, 10 h.

Based on the MTT assay results, further detailed mechanistic studies on cell growth inhibition viz., DNA binding studies, topoisomerase inhibition, apoptotic studies, flow cytometric analysis and molecular docking studies were investigated on the most active derivatives.

2.2.2. *Topoisomerase inhibition and DNA binding studies*

Since, the primary goal of the synthesized novel diindoloazepinone analogues was to serve as possible DNA binding drugs, it is speculated that the investigated compounds have some effect on Topo I and/or II enzyme inhibition which may possibly be through DNA interaction. In the present study, *in vitro* decatenation assay, relaxation assay, topoisomerase IIα-mediated relaxation and DNA cleavage assay, topoisomerase I-mediated relaxation assay, and DNA binding studies such as DNA intercalation assay, circular dichroism and UV-visible spectroscopy were performed on the active compounds **10**, **11** and **13** to evaluate whether their antiproliferative effect was a consequence of the envisioned mechanism of action. Additionally, the effect of the active compound **11** on the viscosity of DNA solution was also studied to ascertain its mode of binding with DNA.

2.2.2.1. Decatenation assay. When topoisomerase acts on catenated circular DNA - kDNA, it catalyzes the release of catenanes and various decatenated forms such as supercoiled and relaxed forms as major products along with the minor products such as open circular, nicked open circular, linear forms. Inhibition of the human topoisomerase IIα will decrease or completely inhibit the decatenated product formation, as a result kDNA will be higher in wells. We used etoposide, a well-known topoisomerase inhibitor, as standard in this procedure. Upon treatment with the investigational compounds, the presence of kDNA in the wells was not observed, indicating that the investigational compounds do not interfere with Topo-IIα enzyme (A, Fig. 3). Fig. 3B depicts the results obtained upon quantification of the

Table 1
In vitro cytotoxicity (IC_{50} values in μM)[a] data for the synthesized compounds.

Code	R^1	R^2	R^3	DU143	HEPG2	RKO	A549	HEK-293
10	–	H	H	13.6 ± 0.23	**8.9 ± 0.56**	12.5 ± 0.56	15.00 ± 0.31	65.3 ± 1.23
11	–	H	CH_3	**6.59 ± 0.35**	**4.89 ± 0.89**	**5.63 ± 0.56**	**4.2 ± 0.02**	**53.6 ± 0.56**
12	–	H	F	**4.77 ± 0.89**	12.9 ± 0.78	**6.3 ± 0.145**	**5.23 ± 0.12**	–
13	–	H	Cl	**4.73 ± 0.25**	**4.8 ± 0.45**	22.1 ± 1.02	**5.23 ± 0.56**	89.6 ± 1.58
14	–	H	Br	38.9 ± 1.25	18.0 ± 0.58	19.16 ± 0.15	15.63 ± 0.89	–
15	–	CH_3	CH_3	11.29 ± 0.89	16.6 ± 0.23	43.94 ± 0.14	14.56 ± 0.12	–
16	H	H	H	10.27 ± 0.78	19.5 ± 0.23	32.09 ± 0.56	**9.6 ± 0.23**	–
17	H	H	CH_3	49.28 ± 1.89	34.5 ± 0.45	35.3 ± 0.56	20.5 ± 0.23	–
18	H	H	F	34.11 ± 0.78	21.7 ± 1.23	18.1 ± 0.45	**6.2 ± 0.125**	–
19	H	H	Cl	14.7 ± 1.2	**4.4 ± 0.89**	**6.8 ± 0.89**	15.2 ± 0.56	–
20	H	H	Br	14.3 ± 0.56	21.2 ± 0.78	27.1 ± 1.4	15.6 ± 0.56	–
21	H	CH_3	CH_3	30.69 ± 0.23	43.67 ± 0.89	33.16 ± 0.56	65.3 ± 1.56	–
22	Cl	H	H	25.6 ± 0.25	21.2 ± 0.12	26 ± 0.45	10.2 ± 0.145	–
23	Cl	H	CH_3	53.5 ± 0.56	27.06 ± 0.55	30 ± 0.589	56.3 ± 0.12	–
24	Cl	H	F	27.9 ± 1.23	14.98 ± 0.12	23.64 ± 0.23	**8.5 ± 0.56**	–
25	Cl	H	Cl	36.05 ± 0.78	17.08 ± 0.56	33 ± 1.23	38.9 ± 0.89	–
26	Cl	H	Br	**6.3 ± 0.89**	18.5 ± 0.52	32 ± 1.58	22.5 ± 0.23	–
27	Cl	CH_3	CH_3	21.2 ± 0.89	24.5 ± 0.78	16.3 ± 0.25	12.3 ± 0.89	–
28	H	H	H	33.68 ± 0.56	35.38 ± 0.89	23.9 ± 1.25	86.3 ± 0.56	–
29	H	H	CH_3	36.9 ± 0.78	46.69 ± 1.89	37.8 ± 0.56	89.6 ± 0.12	–
30	H	H	F	67.4 ± 0.56	30.06 ± 0.45	46.5 ± 0.89	12.5 ± 0.89	–
31	H	H	Cl	25 ± 1.23	31.2 ± 1.02	22.2 ± 1.45	24.2 ± 1.23	–
32	H	CH_3	CH_3	11.4 ± 1.45	12.5 ± 0.22	15.6 ± 0.012	12.63 ± 0.45	–
33	Cl	H	CH_3	31.5 ± 1.235	30.34 ± 0.25	28.9 ± 0.23	15.63 ± 0.56	–
34	Cl	H	F	25.2 ± 1.36	27.5 ± 1.58	31.5 ± 1.78	36.9 ± 1.25	–
Dox[b]	–	–	–	1.23 ± 0.023	2.45 ± 0.012	1.37 ± 0.156	1.23 ± 0.056	9 ± 1.1

The bold indicate compounds with IC50 values < 10 μM.

[a] 50% inhibitory concentration determined by taking the mean value of n = 3 independent MTT assay experiments after 48 h of compound treatment using a non-linear regression analysis. DU143 - prostate cancer cells, HEPG2 - liver carcinoma cells, RKO - colon carcinoma cells, A549 - lung cancer cells, HEK-293 - human embryonic kidney cells.

[b] Dox - doxorubicin.

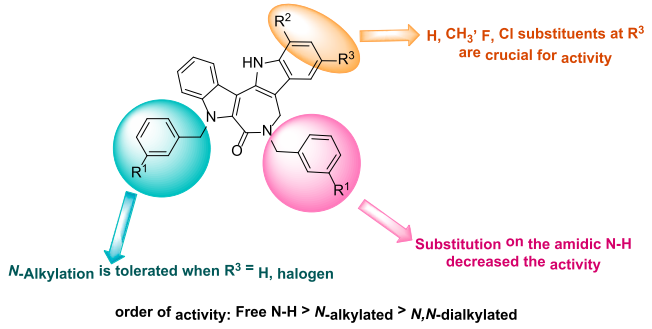

Fig. 2. SAR analysis of diindoloazepinone derivatives.

percent inhibition of decatenation by the investigational compounds in comparison with etoposide. Additionally, densitometric analysis using supercoiled (SC) and relaxed form (Rel.) as decatenation products for relative decatenation was performed (C, Fig. 3). Relative decatenation is the total amount of products formed with 100 ng of DNA. It was found that the products obtained were higher than the standard drug - etoposide, which ultimately support the output obtained from the percentage inhibition of the decatenation assay. The results, thus, indicate the absence of enzyme inhibition. In order to confirm this result, we further performed the relaxation assay for human topoisomerase IIα.

2.2.2.2. Topo IIα-mediated DNA relaxation assay. Topoisomerase II (Topo II) makes nicks in both the strands of the DNA and modifies the topology of the DNA resulting in the initiation of many repair pathways by religating the phosphodiester bonds [31]. Topoisomerase releases the entanglement of the supercoiled DNA and as a result, a large number of relaxed form of DNA were observed on the agarose gel, which migrated more slowly [3,32]. Results of our experiment were compared with etoposide (Topo II inhibitor) as shown in Fig. 4. We witnessed that, in the case of etoposide, supercoiled form was observed as major product, while **10**, **11** and **13** majorly showed the relaxed form of DNA as the major product, thus indicating the investigated compounds are not Topo IIα inhibitors (Fig. 4).

2.2.2.3. Topo IIα-mediated DNA cleavage assay. In order to corroborate the catalytic inhibitory behaviour of our compounds, Topo II cleavage complex assay was performed, which mainly helps in monitoring the ability of compounds to induce the linearization of plasmid DNA in the presence of Topo IIα. Fig. 5 shows that, etoposide, which is a known Topo II poison, strongly induced DNA cleavage thus resulting in the formation of band corresponding to linear form of DNA. Whereas, our investigational compounds do not show the formation of linear band, indicating that the tested compounds have no capacity to poison Topo IIα. The results obtained from the decatenation, relaxation and cleavage complex assays confirm that the compounds have no action on Topo IIα (neither as catalytic inhibitors nor as poisons).

2.2.2.4. Topo I-mediated DNA relaxation assay. Topo I is a known potential target for several clinically used anticancer drugs owing to its involvement in the replication and proliferation process as confirmed by its major expression in actively replicating cells as compared to normal cells. Under normal circumstances, Topo I controls the changes in the DNA topology by cutting single stranded DNA and re-joining the phosphate backbone. Topo I inhibitors act by two mechanisms, either they bind to topoisomerase directly or they may bind to DNA thereby altering its structure, thus, masking it from being recognized by the enzyme. With the confirmation that the investigational compounds do not act as Topo IIα inhibitors or poisons, Topo I relaxation assay was performed taking camptothecin (Topo I inhibitor) as reference standard. When these compounds were incubated with Topo I, we found out that two of our compounds **10** and **11** showed supercoiled form along with some nicked open circular (NOC) form in agarose gel as compared to camptothecin. This clearly

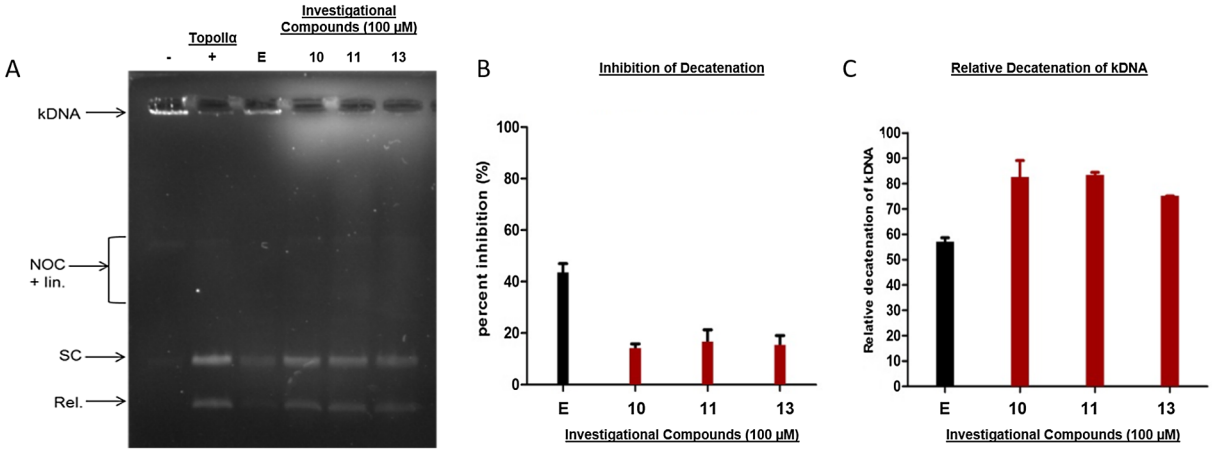

Fig. 3. A. Agarose gel image for the decatenation assay: kDNA (100 ng) was used substrate. kDNA was treated with human topoisomerase IIα along with either etoposide (100 μM) or compounds (100 μM) and decatenation products formed were observed and quantified. 1st lane: kDNA; 2nd lane: kDNA + h Topo IIα 3rd lane: kDNA + h Topo IIα + etoposide (100 μM); lane 4–6: kDNA + h Topo IIα + compounds (100 μM), B. Quantification of kDNA left for percent inhibition of decatenation by investigational compounds. C. Quantification of relative decatenation of kDNA by investigational compounds as compared to etoposide. E: etoposide, NOC: nicked open circular DNA, Lin.: linear form, SC: supercoiled form, Rel.: relaxed form.

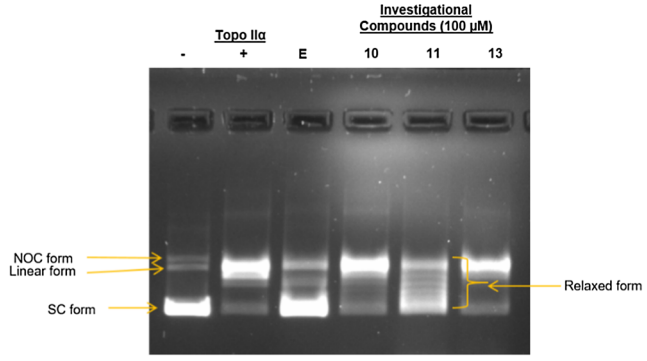

Fig. 4. Relaxation assay for h Topo IIα: pUC19 was used as substrate and incubated with either etoposide (100 μM) or compounds (100 μM) without ethidium bromide. Relaxed DNA as product was observed for relaxation. E: etoposide, NOC: nicked open circular DNA, SC: supercoiled form.

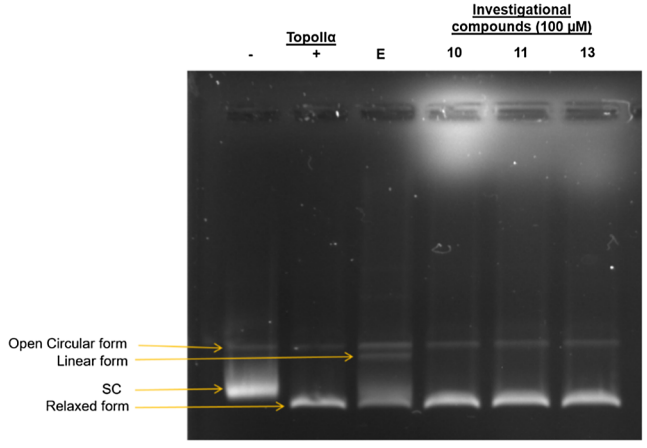

Fig. 5. Stabilization of cleavage complex assay: After treatment with h Topo IIα, negatively supercoiled plasmid was incubated with either 100 μM etoposide or investigational compounds. The agarose gel was run in excess of ethidium bromide to check the formation of linear band. In contrast to etoposide, a linear band was not observed in any of the tested compounds. E: etoposide, SC: supercoiled form.

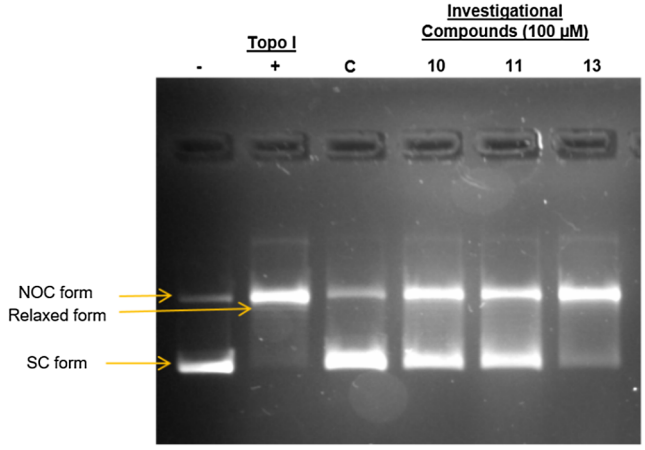

Fig. 6. Relaxation assay for Topo I: Negatively supercoiled DNA pBR322 was used as substrate which was incubated with 100 μM camptothecin or compounds without ethidium bromide. Relaxed DNA as product was observed for relaxation. C: camptothecin, NOC: nicked open circular DNA, SC: supercoiled form.

shows that among the three compounds investigated, **10** and **11** are good and relatively selective inhibitors of Topo I compared to Topo IIα (Fig. 6). Compound **11**, which showed high level of cytotoxicity against all the cell lines screened, also showed high potency against Topo I. However, compound **10**, with relatively low cytotoxicity displayed similar potency against Topo I inhibition. Thus, we cannot exclude the possibility that other pathways might also be targets for this series of compounds, with Topo I inhibition playing a fundamental role in cytotoxicity. We proceeded with DNA binding studies to examine if the investigational compounds bind at the minor groove of the DNA in addition to their interaction with Topo I by trapping the Topo I-DNA cleavage complex by interacting at the cleavage site, which is the mechanism of action of most interfacial poisons, such as camptothecin [2].

2.2.2.5. DNA intercalation assay. Compounds with linear geometry tend to intercalate the DNA and either distort the DNA structure or change its basic structure, thereby, changing the degree of supercoiling

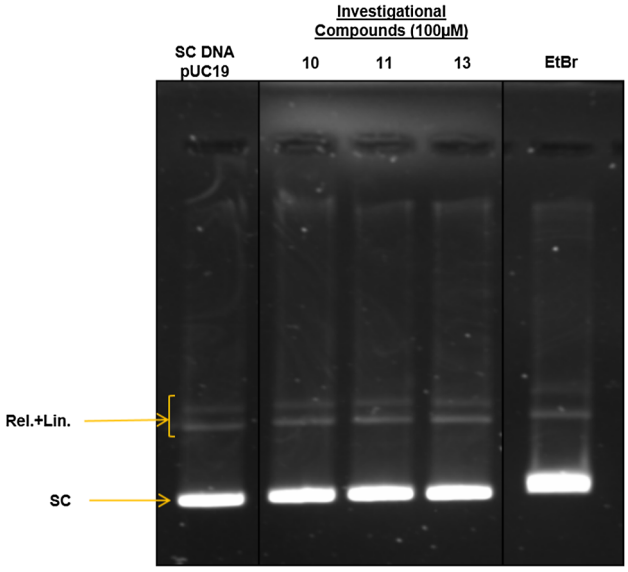

Fig. 7. Intercalation assay: Supercoiled DNA (SC DNA) pUC19 was used as substrate and incubated with either compounds (100 μM) or ethidium bromide (100 μM). SC: supercoiled form, EtBr: ethidium bromide, Lin.: linear form, Rel.: relaxed form.

or mass of the plasmid DNA that could be detected by observing the retardation in migration during electrophoresis. Negatively supercoiled form pUC19 was used as substrate in this assay. It was found that in the presence of ethidium bromide (EtBr), a strong DNA intercalator, there was retardation in the DNA migration during gel electrophoresis (Fig. 7). The investigational compounds, however, have displayed less pronounced retardation in comparison with EtBr, thus indicating that the tested compounds may not be DNA intercalators, but are possible DNA groove binding agents [3,32a,d]. From the decatenation, relaxation and DNA intercalation assays, it is revealed that the investigational compounds (**10**, **11** and **13**) inhibit Topo-I mostly by binding at the interface of Top1cc-DNA complexes by interacting with the minor-groove of the DNA, hence can be considered as good candidates for development as anticancer molecules.

2.2.2.6. Circular dichroism. The primary observation of these novel synthesized compounds as DNA binding agents from the preceding studies, has been further validated for their ability to bring about changes in DNA conformation by employing circular dichroism (CD) as a tool (Fig. 8) [33]. The CD spectrum of ^{CT}DNA, displays positive cotton effect, with a peak at 275 nm and a trough at 245 nm due to base stacking and helicity of B-form of DNA, respectively. Intercalators disrupt both the bands while MGBs do not show major changes in the DNA bands because of the weak electrostatic interactions involved (Fig. S1, supporting information). Looking at the Y-axis values after incubation with different concentrations of investigational compounds **10**, **11** and **13**, it was found that the CD spectra for ^{CT}DNA showed minor changes at 275 nm and 245 nm wavelength. It can be due to minor groove binding or due to the interference in the CD spectra in milieu of ^{CT}DNA.

2.2.2.7. UV-Visible spectroscopy. In UV-visible spectrophotometer, ^{CT}DNA has a characteristic spectrum of the B-form DNA with a λ_{max} at 260 nm. With an increasing concentration of the investigated compound, a change in the absorbance profile is observed indicating DNA binding property (either DNA-intercalating or minor/major groove binding) [34]. When **10**, **11** and **13** were treated with ^{CT}DNA at various concentrations, a weak hypochromicity (decrease in absorbance) without bathochromic shift was observed, which is consistent with minor groove binding, indicating the compounds have DNA groove binding capability and thus impede the incoming wavelength causing changes in the absorption spectrum [34,35] (Fig. 9). The minor groove binding mode of the most active compound **11**, was further confirmed by viscosity studies [35] (Fig. S2, supporting information).

2.2.3. Apoptotic studies

2.2.3.1. Morphological observations. Apoptosis is typically characterized by cell death-related biochemical and morphological changes. In this study, to investigate whether the cell death was induced by apoptosis, A549 cells were treated with various concentrations (0, 1, 2.5, 5 and 10 μM) of our most active compound **11**. After 48 h of incubation, images were captured in phase contrast microscopy which are depicted in Fig. 10A, wherein, characteristic morphological features like the shrinkage of cells, deformation of cell wall, detachment from substratum, reduction in the number of viable cells were observed in a dose-dependent manner as compared to the control, clearly indicating apoptosis.

2.2.3.2. Acridine Orange/Ethidium bromide (AO/EB) staining. Dual acridine orange/ethidium bromide (AO/EB) fluorescent staining which is visualized under a fluorescent microscope, can be used to identify apoptosis-associated changes in cell membrane during apoptosis. It is also effective in precisely distinguishing cells in different stages of apoptosis. AO penetrates normal and early apoptotic cells with intact membranes, fluorescing green when bound to DNA, while EB only enters cells with damaged membranes, such as late apoptotic cells and dead cells, and binds to concentrated DNA fragments or apoptotic bodies thus emitting orange-red fluorescence [36]. It can be construed from Fig. 10B that control cells maintained their normal morphology and appeared green in colour and on the contrary, the cells treated with our compound **11** showed green fluorescence as that of control but with morphological changes like

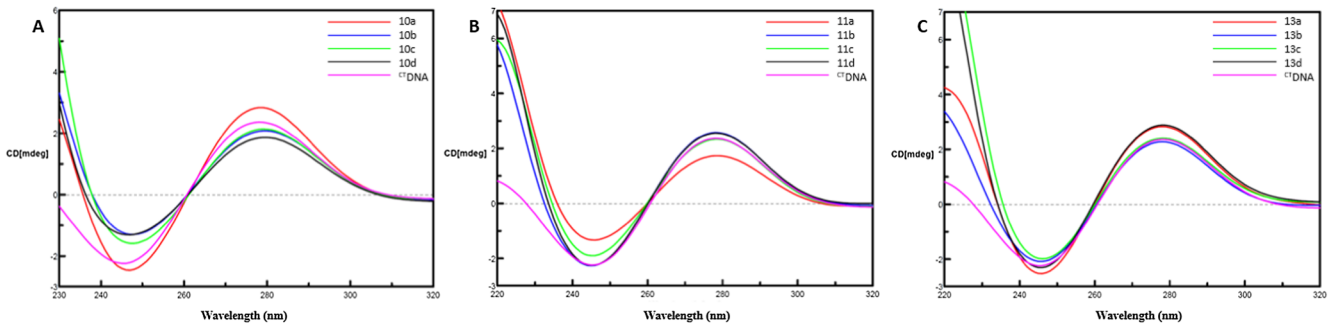

Fig. 8. CD spectra of ^{CT}DNA with various concentrations of compounds **10** (A), **11** (B) and **13** (C), where a: Compound/DNA = 1/10 ratio, b: 1/6, c: 1/4, d: 1/3 and ^{CT}DNA: ^{CT}DNA in Tris-HCl buffer (pH-7.4).

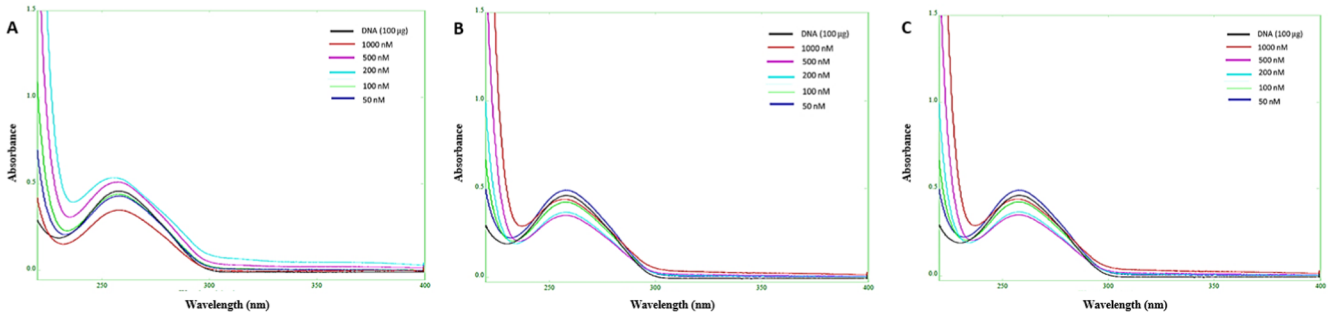

Fig. 9. UV-Vis Spectra with ^{CT}DNA (100 µg) with various concentration of investigational compounds **10** (A), **11** (B) and **13** (C).

cell shrinkage, membrane blebbing, condensation of chromatin and apoptotic body formation indicating that the compound induces dose-dependent apoptosis in A549 cells.

2.2.3.3. DAPI nucleic acid staining. 4′-6-Diamidino-2-phenylindole (DAPI), a fluorescent dye, pervades intact membrane of live cells and stains the nucleus light blue, whereas, the apoptotic cell nuclei appears as bright blue due to chromatin condensation. To further examine the nuclear morphological changes in A549 cells, DAPI staining was performed after 48 h of treatment with compound **11**. In this investigation, it was noticed that the control cells were intact with normal morphology, while those treated with compound **11** at concentrations 1, 2.5, 5 and 10 µM displayed nuclear changes like horse-shoe shaped, irreversible chromatin condensation and fragmented bright nuclei. From the results, it was evident that the compound **11** had induced apoptosis in A549 cells (Fig. 10C).

2.2.4. Flow cytometric analysis

2.2.4.1. Effect of mitochondrial membrane potential ($\Delta\psi_m$). Changes in the mitochondrial membrane potential ($\Delta\psi_m$) as a result of mitochondrial dysfunction have been originally postulated to be an obligate event in the intrinsic apoptotic signalling pathway [37]. As a consequent outcome of apoptosis, opening of the mitochondrial permeability transition pore is observed which induces depolarization of the transmembrane potential ($\Delta\psi_m$), release of apoptogenic factors and loss of oxidative phosphorylation. To evaluate the effect of compound **11** on mitochondria, A549 cells were initially treated with compound **11** at concentrations 1, 2.5, 5 and 10 µM and were further stained with a lipophilic cationic dye JC-1, in which normal polarized mitochondria stains red due to formation of J-aggregates and green color was observed for depolarized mitochondria of apoptotic cells due to formation of J-monomers.

Flow-cytometric analysis of the treated cells clearly showed remarkable increase in the mitochondrial membrane depolarisation as compared to the control cells, as a result, increase in depolarised cell population (*P*2) in a concentration dependent manner (Fig. 11) from 4.44% in control to 47.81% at 5 µM. This dose-dependent increase in depolarised cell population is represented as bar graph (Fig. S3, supporting information). This assay further suggested the involvement of mitochondria-dependent apoptotic pathway in the mechanism of action of the lead compound **11**.

2.2.4.2. Cell cycle analysis. Cell cycle arrest displayed by the cytotoxic compounds can be analysed by cell cycle analysis. Flow cytometric analysis of cell distribution was performed on the A549 human lung cancer cells treated with compound **11** for 48 h and further stained with propidium iodide dye that is generally excluded from viable cells [38]. According to the analysis results given below, it was evident that compound **11** treatment induces apoptosis cell death, which was corroborated by the appearance of the characteristic sub-diploid DNA content peak (sub-G1). Fig. 12 shows the relative percentages of A549 cells in each phase of the cell cycle following the treatment. We noticed

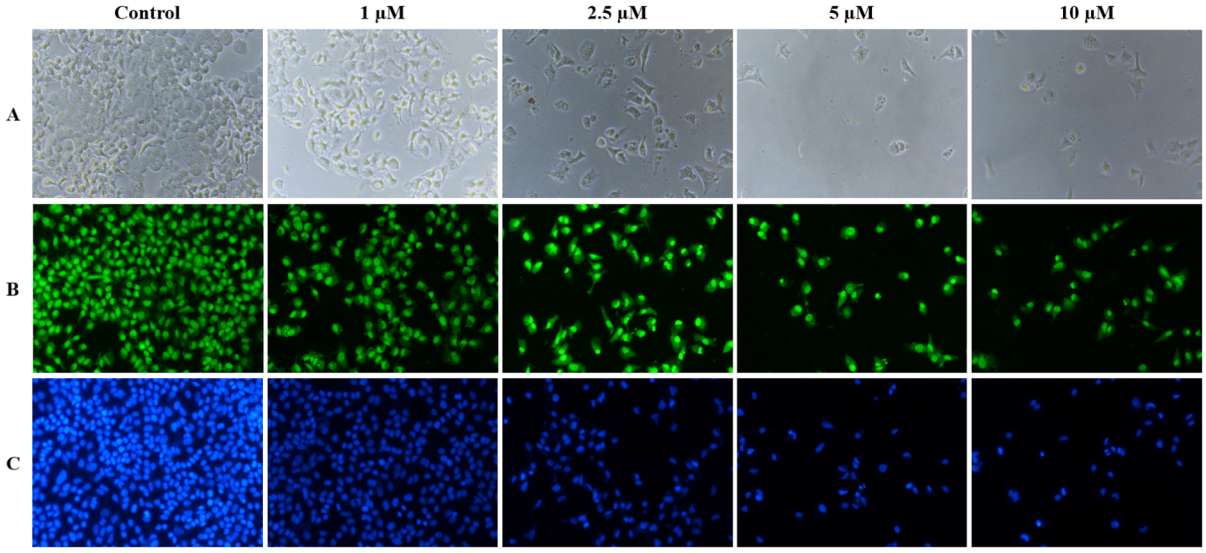

Fig. 10. A) Morphological changes observed in A549 cells treated with the compound **11** at concentrations of 0, 1, 2.5, 5 and 10 µM. After 48 h, the images were captured with a phase contrast microscope at 200X magnification. B) AO/EB staining in A549 cells treated with, 1, 2.5, 5 and 10 µM concentrations of compound **11** for 48 h and compared with control. The images were captured with fluorescence microscope at magnification of 200X. C) DAPI staining images displaying the nuclear morphology of A549 cells treated with compound **11** at concentrations 0, 1, 2.5, 5 and 10 µM for 48 h. The images were captured with fluorescence microscope at magnification of 200X.

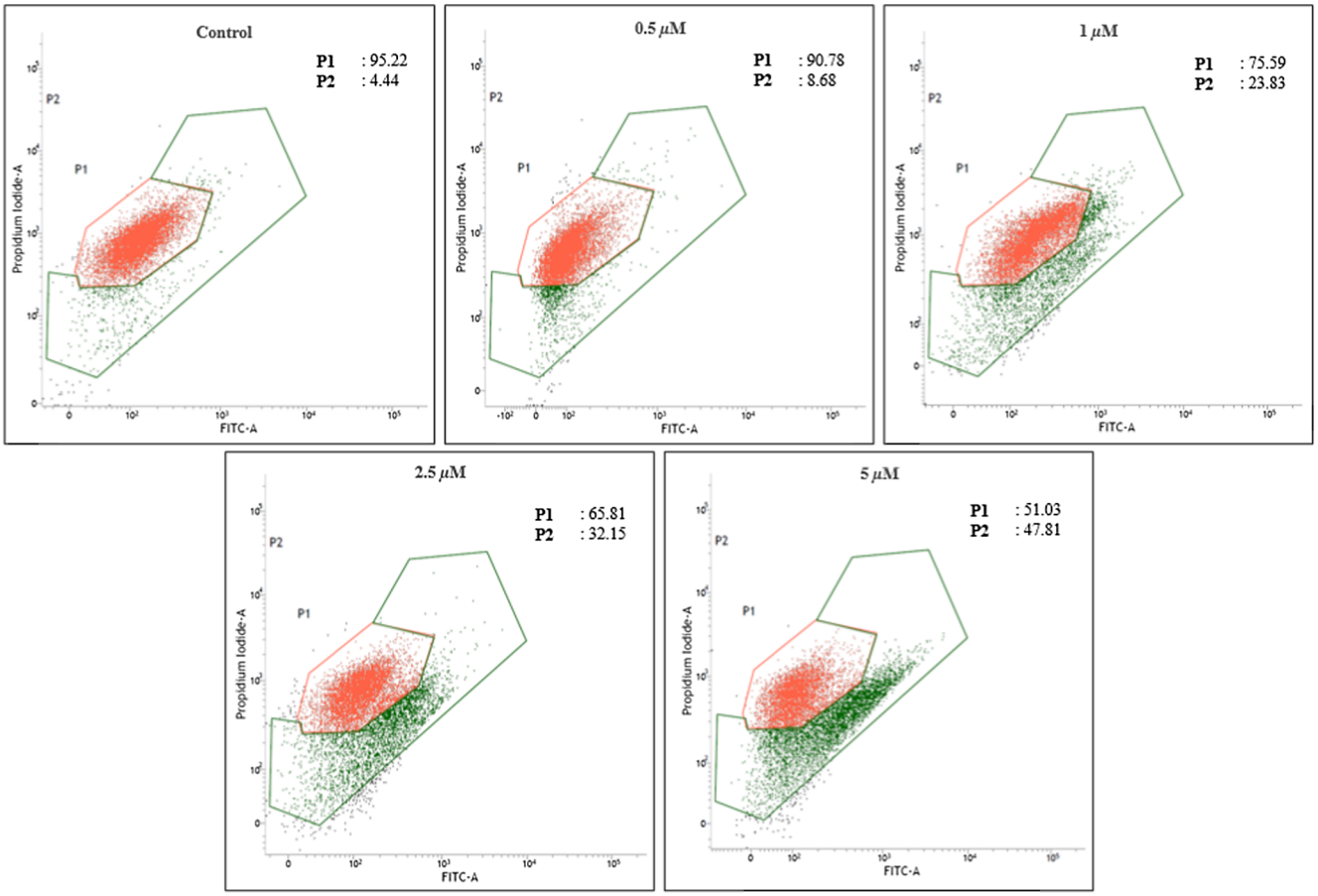

Fig. 11. Effect of compound **11** on mitochondrial membrane potential ($\Delta\psi_m$). A549 cells were treated with the lead compound **11** for 48 h and JC-1 staining was performed on these treated cells along with the control (untreated cells). *P*1 represents formation of J-aggregates in healthy mitochondria, whereas *P*2 represents depolarised mitochondria in cells due to the presence of J-monomers.

that the untreated control cell population showed 2.47% cells in sub-G1 phase, whereas compound **11** treatment resulted in an increase in sub-G1 population from 8.68 to 22.07% with increasing concentrations from 0.5 to 5 μM, thus, demonstrating rise in apoptotic cells. The dose-dependent blockade of sub-G1 phase is also represented as bar diagram in Fig. S4, supporting information.

2.2.4.3. Annexin V-FITC/PI assay. The quantification of apoptotic cell death can be carried out by performing annexin V-FITC/PI assay by using flow cytometry. One of the most commonly used cytofluorometric stains is fluorochrome-labeled annexin V, which binds to the negatively charged phosphatidylserine (PS) exposed on the outer cell membrane, a hallmark of apoptosis, thereby giving fluorescence. Propidium iodide

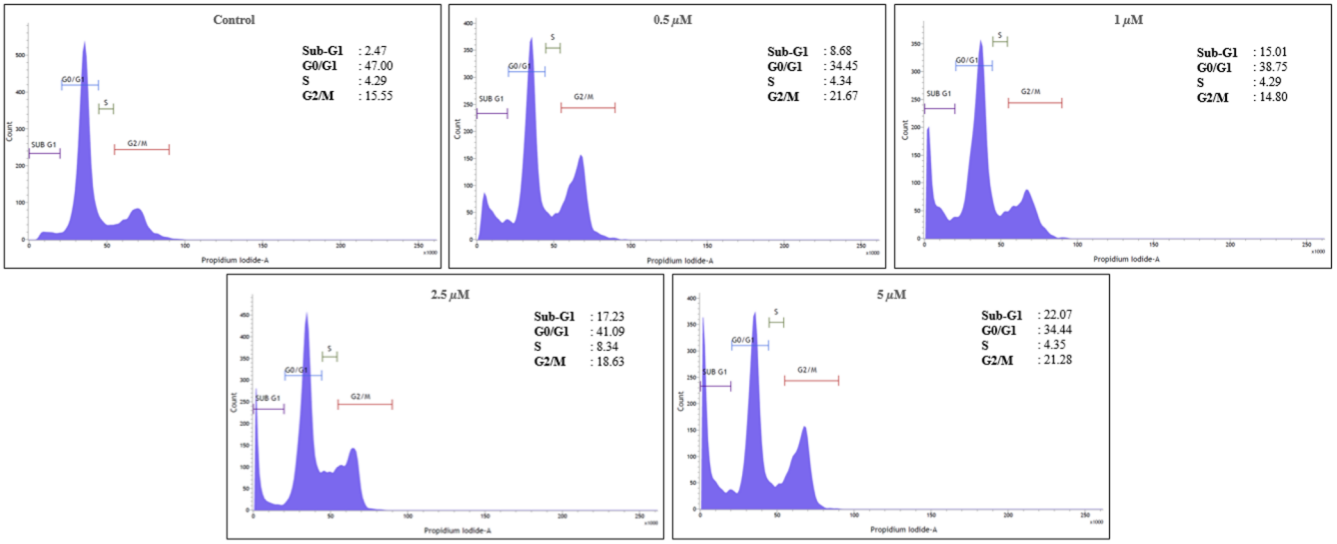

Fig. 12. Effect of compound **11** on cell cycle phase distribution of A549 cells examined by performing cell cycle analysis assay using propidium iodide staining method. The assay was carried out after 48 h of treatment with compound **11** at various concentrations of 0.5, 1, 2.5 and 5 μM along with control (untreated cells).

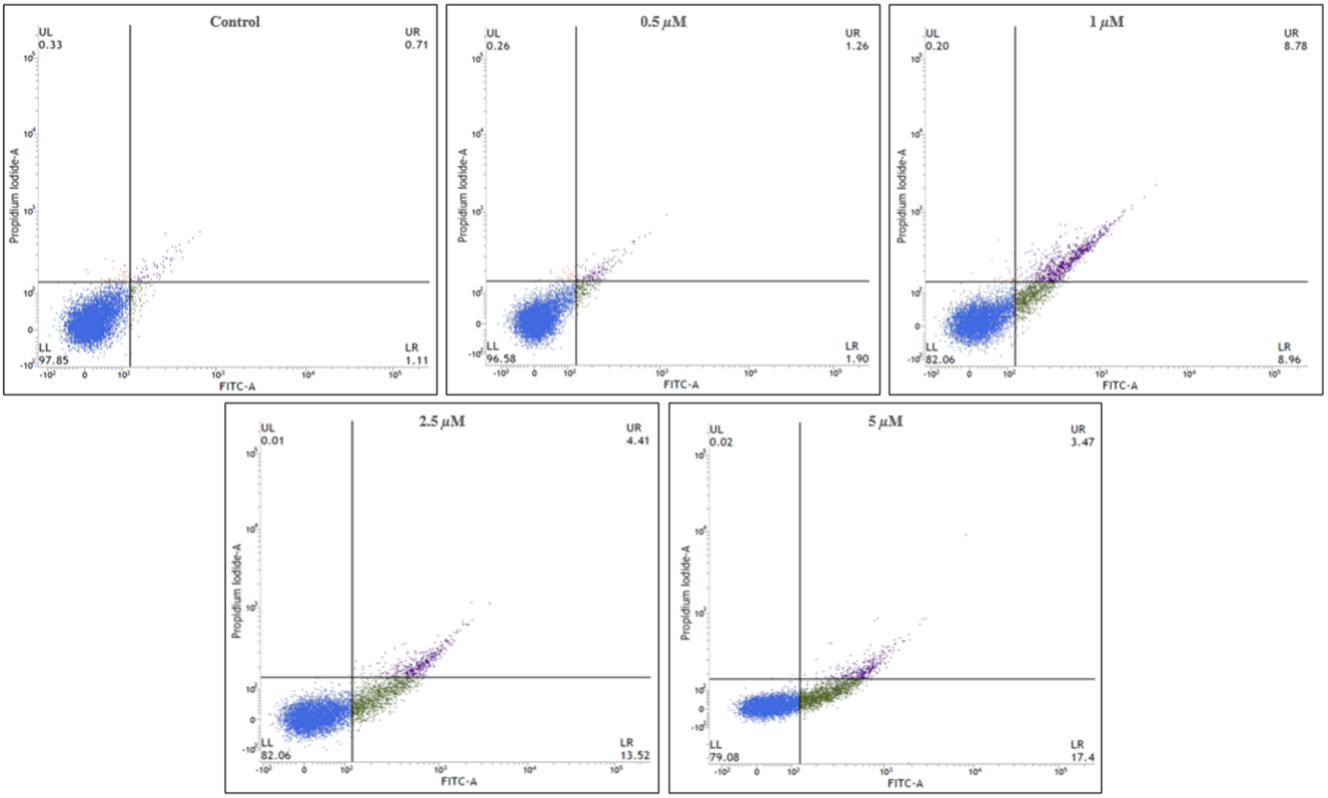

Fig. 13. Effect of compound on cell apoptosis as measured by annexin V/propidium iodide staining assay. A549 cells were treated with different concentrations of compound **11** ranging from 0.5 to 5 μM for 48 h. Then 10,000 cells from each treated sample and control were harvested and labelled with annexin V-FITC and PI. The percentage of cells in each stage of cell apoptosis were quantified by flow cytometry and is represented inside four quadrants, i.e. upper left quadrant shows the necrotic cells; bottom left quadrant represents live cells, while the bottom right quadrant represents early apoptotic cells and the upper right quadrant indicates late-apoptotic cells.

(PI), a widely used non-specific, phenanthrene-containing DNA intercalating agent, is excluded by the plasma membrane of living cells. Thus, cells which stained positive for annexin V-FITC/PI represent those in the late apoptotic stage that have lost membrane integrity [39]. Cells in different stages, such as, necrotic cells (Q1-UL; AV-/PI +), live cells (Q2-LL; AV-/PI-), early apoptotic cells (Q3-LR; AV + /PI-), and late apoptotic cells (Q4- UR; AV + /PI +) can be detected using annexin assay. A549 cells upon treatment with compound **11** at varied concentrations (1, 2.5, 5 and 10 μM) have shown increased binding to the annexin V-FITC/PI indicating dose-dependent cellular apoptosis. The percentage of early apoptotic cells (AV + /PI-) showed and dose-dependent increase after treatment with different concentrations of compound **11** for 48 h, in comparison to the control cells (Fig. 13). Graphical representation of the results is depicted in Fig. S5 (supporting information).

2.3. Molecular docking

Topotecan, a Topo I poison, was re-docked into the Topo I active site (PDB: 1K4T) to validate the docking protocol (Fig. S6, supplementary information), which showed hydrogen bonding with Arg364, Lys532 and Asp533 (A, Fig. 14). After the validation of the docking protocol, we have performed molecular docking studies on compound **11** which showed hydrogen bond with Gln633 and Ala635 along with hydrophobic interactions with Ile535 and π-cation interaction with Arg364 (B, Fig. 14). It can be seen that both topotecan and compound **11** bind at the site surrounded by amino acid residues like Asp533, Thr718 and Arg364 which suggested that our compound **11** also lodged at the active site of Topo I in a comparable manner as that of the co-crystal.

In order to examine and understand the DNA-binding property of the most active molecule **11** amongst the library of synthesized molecules, *in silico* studies were carried out using three-dimensional crystal structure of AT-rich A-tract DNA dodecamer d(CGCAAATTT GCG) complexed with minor-groove binding drug: Hoechst 33258. The co-crystal, Hoechst, when re-docked showed hydrogen bonding with dT7A and dT8A (A, Fig. 15), thus validating our docking protocol (Fig. S7, supplementary information). Similarly, compound **11** also aligned itself in the minor groove like the co-crystal and displayed hydrogen bonds with dT9A and dG10A (B, Fig. 15). From the docking results, it was observed that the compound **11** gets excellently aligned along the minor groove, akin to Hoechst 33,258 (C, Fig. 15), This indicates the possible binding capability of our compound at the interface of Topo I and DNA thus, supporting the results obtained from the *in vitro* biological assays.

3. Conclusion

In conclusion, a new series of diindoloazepinone analogues were designed, synthesized and further evaluated for their *in vitro* cytotoxic potential against different cancer cell lines and also a non-cancerous immortalized human embryonic kidney cells. The results of this preliminary cytotoxicity screening using the MTT assay suggested that most of the compounds showed good activity and the most potent one, **11**, displayed a broad spectrum of activity against all the tested cancer cell lines specifically in A549 (lung cancer cells) with IC_{50} value of 4.2 μM. Interestingly, it showed a 13-fold selectivity upon the non-cancerous immortalized human embryonic kidney cells. Further detailed biological studies including cell cycle analysis, DNA binding studies, Topo I inhibition, circular dichroism, UV-visible spectroscopy, viscosity studies, apoptotic studies and flow cytometric analysis delivered promising results. The flow cytometric analysis revealed that these derivatives caused cell cycle arrest at sub-G1 phase. Furthermore, it

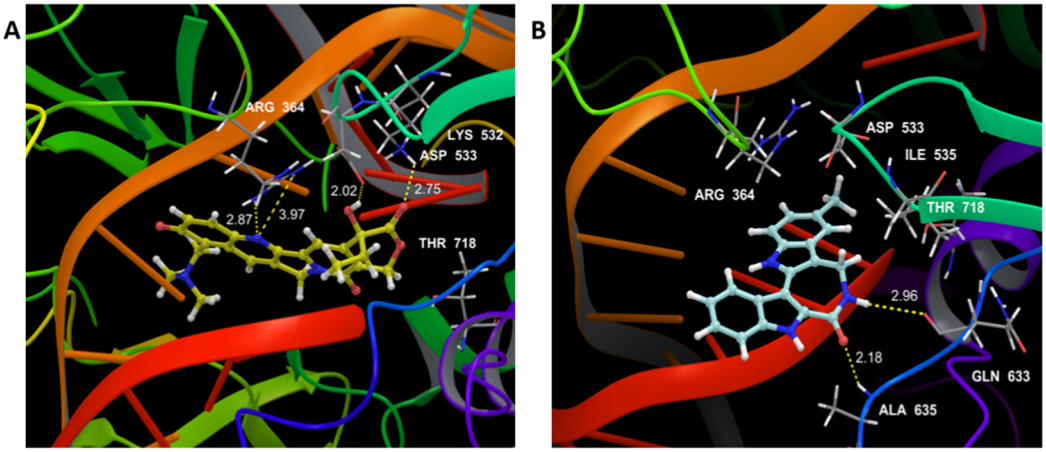

Fig. 14. A and B represent the binding pose, hydrogen bonds (yellow dotted lines) and hydrophobic interactions of topotecan (co-crystal) and compound **11** with Topo I (PDB code: 1K4T). The co-crystal and compound **11** are indicated as yellow and turquoise ball and stick models, respectively. Hydrogen bonding is indicated by yellow dotted line.

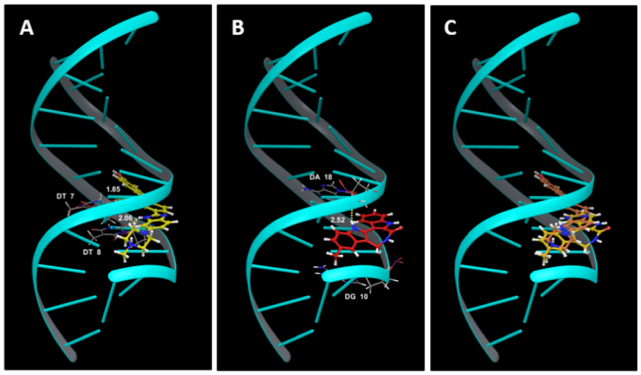

Fig. 15. A and B represent minor groove binding of co-crystal, Hoechst 33258, and compound **11** into d(CGCAAATTTGCG) (DNA) (PDB code: 264D), respectively. DNA is represented as a turquoise ribbon, while the co-crystal is indicated in yellow and compound **11** is represented as red colored ball and stick models. C shows the superimposition of Hoechst (orange) and compound **11** (mustard yellow) along the minor groove of DNA. The yellow dotted lines indicate hydrogen bonding.

forms a stable complex with efficient binding to the minor groove of DNA, they can effectively and, most importantly, selectively inhibit Topo I without having an effect on Topo IIα. Molecular docking studies also showed that the interactions of **11** matched well with the co-crystal, Hoechst, which is indicative of minor-groove binding into DNA. It also showed good interactions with Topo I, thus, implying its possible mechanism of action as interfacial Topo 1 inhibition *via* minor groove binding.

4. Experimental section

4.1. General procedures

Reagents and solvents were purchased from commercial sources. All the reactions were monitored routinely by thin layer chromatography (TLC) performed on MERCK silica gel 60-F254 (0.5 mm) pre-coated aluminium plates and visualized using ultraviolet light or by treatment with iodine or anisaldehyde dip. Column chromatography was performed by using silica gel (60–120). Evaporation of the solvents was performed under reduced pressure by using a rotary evaporator below 45 °C. ^{1}H and ^{13}C NMR spectra were recorded with a Bruker 500 MHz instrument in $CDCl_3$ or [d_6] DMSO solvent with tetramethylsilane as the internal standard. Chemical shifts for ^{1}H and ^{13}C are reported in parts per million (ppm) downfield from tetramethylsilane. Spin multiplicities are described as s (singlet), brs (broad singlet), d (doublet), t (triplet), q (quartet) and m (multiplet). Coupling constant (*J*) values are reported in hertz (Hz). HRMS was performed with an Agilent QTOF mass spectrometer 6540 series instrument. Melting points were determined using an electrothermal digital melting point apparatus digital melting point apparatus IA9100. Infrared spectra (IR) were recorded on a Perkin Elmer 1600 series FTIR spectrometer. The names of all the compounds given in the experimental section were taken from ChemBioDraw Ultra, Version 14.0.

4.2. Chemistry

4.2.1. 3-(1H-Indole-2-carboxamido)propanoic acid *4*

To a solution of β-alanine ethyl ester hydrochloride **2** (1 equiv) in DMF (50 mL) under nitrogen atmosphere was added indole-2-carboxylic acid **1** (31 mmol), followed by anhydrous DMAP (2.2 equiv) and finally EDCI·HCl (2 equiv) at 0 °C. The reaction was allowed to stir at 0 °C for 4 h and continued at room temperature till the completion of the reaction (20 h). To the reaction mixture, was added crushed ice and stirred continuously to obtain solid. The solid intermediate was filtered, exhaustively washed with water and the solid was dried under vacuum to obtain the desired ester intermediate **3** as white solid (90%). This ester was dissolved in EtOH and NaOH (3 equiv) was added and the reaction mixture was allowed to stir for 30 min at rt. After the completion of the reaction, the solvent was evaporated under vacuum and water was added. To this, 1 N HCl was added slowly until acidic and the precipitate was filtered and dried to obtain the acid **4** (92%).

4.2.2. 3,4-Dihydro-2H,10H-azepino[3,4-b]indole-1,5-dione *5*

In methanesulfonic acid (1 equiv) was dissolved phosphorus pentoxide (1.2 equiv) and heated to 80 °C. Once homogenous, carboxylic acid **5** (0.76 mmol) was added, the reaction stirred and monitored by TLC until complete. The reaction was quenched with ice and exhaustively extracted with ethyl acetate. The combined organic extractions were dried (Na_2SO_4) and concentrated under vacuum to afford the desired intermediate **5** as a solid (60%)

4.2.3. 10-Benzyl-3,4-dihydroazepino[3,4-b]indole-1,5(2H,10H)-dione *7a*

To a solution of indoloazepinone **5** (2.33 mmol) in DMF (5 mL) maintained at 0 °C was added K_2CO_3 (3 equiv) was stirred for 15 min. To this, benzylbromide **6a** (1 equiv) was added dropwise and the reaction mixture was refluxed for 8 h. After the completion of the reaction (TLC), the reaction mixture was cooled to rt and was poured onto crushed ice. Further extraction with EtOAc and concentration of the

dried organic layers followed by purification with column chromatography yielded the desired *N*-alkylated indoloazepinone **7a** as pale yellow solid (92%); MP: 166–168 °C. IR (neat): ν_{max} 3191, 3058, 1645, 1504, 1449, 1449, 1377, 1313, 1253, 1199, 749, 728, 692, 543 cm^{-1}; ^1H NMR (500 MHz, DMSO) δ 8.90 (t, J = 6.0 Hz, 1H), 8.30 (d, J = 7.4 Hz, 1H), 7.58 (d, J = 8.2 Hz, 1H), 7.37–7.31 (m, 2H), 7.31–7.29 (m, 1H), 7.28 (d, J = 7.5 Hz, 2H), 7.22 (t, J = 7.3 Hz, 1H), 7.13 (d, J = 7.1 Hz, 2H), 5.91 (s, 2H), 3.43 (dd, J = 10.6, 5.7 Hz, 2H), 2.84 (dd, J = 6.6, 3.8 Hz, 2H). ^{13}C NMR (125 MHz, DMSO) δ 196.5, 162.9, 138.3, 138.0, 134.6, 129.0, 127.7, 127.0, 125.8, 125.3, 123.8, 123.3, 116.1, 112.1, 48.2, 45.5, 37.1. HRMS (ESI): *m/z* calcd for $C_{19}H_{16}N_2O_2$ 305.1285; found 305.1289 $[M+H]^+$.

4.2.4. 10-(3-Chlorobenzyl)-3,4-dihydroazepino[3,4-b]indole-1,5(2H,10H)-dione **7b**

According to the procedure described for the synthesis of **7a**, **7b** was prepared from **5** and **6b** in 89% yield as pale yellow solid; MP: 177–179 °C. IR (neat): ν_{max} 3183, 1661, 1644, 1599, 1578, 1505, 1461, 1428, 1381, 1260, 800, 745, 773, 680, 561 cm^{-1}; ^1H NMR (500 MHz, $CDCl_3$) δ 8.52–8.50 (m, 1H), 7.40–7.36 (m, 2H), 7.35–7.33 (m, 1H), 7.21 (s, 1H), 7.18 (d, J = 7.9 Hz, 1H), 7.12 (s, 1H), 6.97 (d, J = 6.5 Hz, 1H), 6.91 (s, 1H), 5.84 (s, 2H), 3.58 (dd, J = 10.9, 6.1 Hz, 2H), 2.98–2.96 (m, 2H). ^{13}C NMR (125 MHz, $CDCl_3$) δ 195.5, 163.6, 139.4, 138.3, 134.7, 132.4, 130.0, 127.8, 126.7, 126.3, 125.5, 124.7, 124.1, 117.3, 110.7, 48.3, 45.1, 37.7. HRMS (ESI): *m/z* calcd for $C_{19}H_{15}ClN_2O_2$ 339.0895; found 339.0898 $[M+H]^+$.

4.2.5. 2,10-Dibenzyl-3,4-dihydroazepino[3,4-b]indole-1,5(2H,10H)-dione **8a**

To a solution of indoloazepinone **5** (2.33 mmol) in DMF (5 mL) maintained at 0 °C under nitrogen atmosphere was added NaH (2 equiv) was stirred for 30 min. To this benzylbromide **6a** (2 equiv) was added dropwise and the reaction mixture was allowed to stir at rt for 12 h. After the completion of the reaction (TLC), the reaction mixture was poured onto crushed ice and acidified with 1 N HCl and then extracted with EtOAc followed by purification with column chromatography yielding the *N,N*-dialkylated indoloazepinone **8a** as semi-solid in 90% yield. IR (neat): ν_{max} 1739, 1641, 1505, 1429, 1392, 1355, 1246, 1151, 741, 698, 537 cm^{-1}; ^1H NMR (500 MHz, $CDCl_3$) δ 8.42 (dd, J = 6.6, 2.1 Hz, 1H), 7.43 (dd, J = 6.9, 1.9 Hz, 1H), 7.40–7.31 (m, 2H), 7.30–7.27 (m, 6H), 7.11 (dd, J = 6.2, 2.7 Hz, 4H), 5.90 (s, 2H), 4.81 (s, 2H), 3.60 (s, 2H), 2.79 (dd, J = 5.6, 4.7 Hz, 2H). ^{13}C NMR (125 MHz, $CDCl_3$) δ 195.8, 161.6, 138.4, 137.7, 136.6, 134.1, 128.9, 128.8, 128.0, 127.8, 127.6, 126.7, 125.8, 125.1, 123.8, 123.5, 116.3, 110.6, 50.3, 48.6, 44.1, 43.6. HRMS (ESI): *m/z* calcd for $C_{26}H_{22}N_2O_2$ 395.1754; found 395.1754 $[M+H]^+$.

4.2.6. 2,10-Bis(3-chlorobenzyl)-3,4-dihydroazepino[3,4-b]indole-1,5(2H,10H)-dione **8b**

According to the procedure described for the synthesis of **8a**, **8b** was prepared from **5** and **6b** in 86% yield as semi-solid. IR (neat): ν_{max} 1751, 1573, 1475, 1455, 1428, 1394, 1272, 1095, 992, 873, 741, 562, 550 cm^{-1}; ^1H NMR (500 MHz, $CDCl_3$) δ 8.43 (d, J = 7.3 Hz, 1H), 7.42–7.33 (m, 3H), 7.31–7.26 (m, 2H), 7.26–7.19 (m, 4H), 7.13 (s, 1H), 7.01 (dd, J = 15.0, 7.3 Hz, 2H), 5.85 (s, 2H), 4.79 (s, 3H), 3.66 (s, 2H), 2.84 (dd, J = 5.7, 4.6 Hz, 2H). ^{13}C NMR (125 MHz, $CDCl_3$) δ 195.4, 163.6, 139.4, 138.3, 134.7, 132.4, 130.0, 127.8, 126.7, 126.3, 125.5, 124.7, 124.1, 124.1, 117.3, 110.7, 48.3, 45.1, 37.7, 29.7. HRMS (ESI): *m/z* calcd for $C_{26}H_{20}Cl_2N_2O_2$ 463.0975; found 463.0969 $[M+H]^+$.

4.2.7. 5,7,8,13-Tetrahydro-6H-azepino[3,4-b:5,6-b']diindol-6-one **10**

A mixture of indoloazepinone **5** (0.5 mmol) and arylhydrazine hydrochloride (1.5 equiv) was refluxed in glacial acetic acid (2 mL) and ethanol (2 mL). After stirring at 70 °C for 1 h, the reaction mixture was cooled to rt. Concentrated HCl (0.1–0.5 mL) was added and stirring is continued at 70 °C for 7 h. Reaction was monitored by TLC. After cooling to rt, the reaction mixture was poured into a 5% sodium acetate solution (15 mL). The mixture was extracted with EtOAc and concentrated in vacuo. The residue was purified by silica gel column chromatography, eluted with ethyl acetate:hexane (30:70) to afford the desired product **10.** Yield 54%, yellow solid; MP: 115–117 °C. IR (neat): ν_{max} 3381, 3221, 1631, 1487, 1451, 1315, 1259, 742, 686, 442, 410 cm^{-1}; ^1H NMR (500 MHz, $CDCl_3$) δ 9.81 (s, 1H), 8.79 (s, 1H), 8.04 (d, J = 8.0 Hz, 1H), 7.60 (d, J = 7.6 Hz, 1H), 7.51 (d, J = 7.7 Hz, 1H), 7.45 (d, J = 8.3 Hz, 1H), 7.38 (t, J = 7.3 Hz, 1H), 7.28 (m, 1H), 7.25–7.18 (m, 2H), 6.41 (s, 1H), 4.44 (d, J = 4.9 Hz, 2H). ^{13}C NMR (125 MHz, $CDCl_3$): δ165.0, 137.5, 137.0, 136.4, 132.8, 125.9, 125.9, 123.8, 122.3, 121.6, 120.8, 120.6, 117.8, 112.7, 111.8, 111.4, 109.6, 36.5; HRMS (ESI): *m/z* calcd for $C_{18}H_{13}N_3O$ 288.1131; found 288.1139 $[M+H]^+$.

4.2.8. 10-Methyl-5,7,8,13-tetrahydro-6H-azepino[3,4-b:5,6-b']diindol-6-one **11**

Starting from **5**, compound **11** was obtained as golden yellow solid using a similar procedure as **10**. Yield 63%; MP: 142–145 °C; IR (neat): ν_{max} 3267, 2922, 2862, 1747, 1624, 1489, 1334, 1307, 743, 441, 405 cm^{-1}; ^1H NMR (500 MHz, $CDCl_3$) δ 9.47 (s, 1H), 8.57 (s, 1H), 8.05 (d, J = 7.8 Hz, 1H), 7.51 (d, J = 8.3 Hz, 1H), 7.44–7.41 (m, 1H), 7.40 (s, 1H), 7.37 (s, 1H), 7.33–7.27 (m, 1H), 7.09–7.04 (m, 1H), 6.21 (s, 1H), 4.45 (d, J = 5.1 Hz, 2H), 2.49 (s, 3H);^{13}C NMR (125 MHz, $CDCl_3$): δ 165.1, 140.4, 136.5, 135.3, 132.9, 129.9, 126.1, 125.9, 123.9, 123.8, 121.5, 120.9, 120.7, 117.5, 112.7, 111.1, 109.2, 36.5, 21.6; HRMS (ESI): *m/z* calcd for $C_{18}H_{13}N_3O$ 302.1288; found 300.1286 $[M+H]^+$.

4.2.9. 10-Fluoro-5,7,8,13-tetrahydro-6H-azepino[3,4-b:5,6-b']diindol-6-one **12**

Starting from **5**, compound **12** was obtained as golden yellow solid using a similar procedure as **10**. Yield 47%; MP: 150–153 °C. IR (neat): ν_{max} 3404, 3216, 2970, 1743, 1611, 1484,1452, 1256, 1156, 934, 792, 747, 548, 437, 405 cm^{-1}; ^1H NMR (500 MHz, $CDCl_3$ + DMSO) δ 11.72 (s, 1H), 11.39 (s, 1H), 8.44 (d, J = 8.0 Hz, 1H), 7.86 (s, 1H), 7.82 (d, J = 8.3 Hz, 1H), 7.77–7.67 (m, 2H), 7.57 (t, J = 7.4 Hz, 1H), 7.47–7.40 (m, 1H), 7.09 (dt, J = 9.2, 2.3 Hz, 1H), 4.56 (d, J = 5.0 Hz, 2H). ^{13}C NMR (125 MHz, $CDCl_3$) δ 164.5, 160.30 (d, J = 203.80 Hz), 136.3, 134.3, 133.5, 129.1, 125.5 (d, J = 9.56 Hz), 124.5, 123.1, 121.2, 120.1, 112.3, 112.1 (d, J = 9.33 Hz), 110.5, 108.9, 108.8, 108.5, 101.6 (d, J = 23.52 Hz), 35.5; HRMS (ESI): *m/z* calcd for $C_{18}H_{12}FN_3O$ 306.1037; found 306.1044 $[M+H]^+$.

4.2.10. 10-Chloro-5,7,8,13-tetrahydro-6H-azepino[3,4-b:5,6-b']diindol-6-one **13**

Starting from **5**, compound **13** was obtained as pale yellow solid using a similar procedure as **10.** Yield 44%; MP: 133–135 °C. IR (neat): ν_{max} 3013, 2894, 1634, 1529, 1313, 1151, 1033, 442, 407 cm^{-1}; ^1H NMR (500 MHz, $CDCl_3$ + DMSO) δ 11.35 (s, 1H), 11.18 (s, 1H), 8.21 (d, J = 7.3 Hz, 1H), 7.60 (d, J = 8.0 Hz, 1H), 7.55 (s, 1H), 7.48 (d, J = 8.2 Hz, 1H), 7.41–7.32 (m, 2H), 7.30–7.20 (m, 1H), 7.07 (d, J = 7.9 Hz, 1H), 4.36 (s, 2H). ^{13}C NMR (125 MHz, $CDCl_3$ + DMSO) δ 164.2, 136.3, 135.3, 134.1, 129.6, 126.3, 124.4, 124.3, 123.0, 121.2, 120.4, 120.0, 116.2, 112.6, 112.4, 110.0, 108.5, 35.1; HRMS (ESI): *m/z* calcd for $C_{18}H_{12}ClN_3O$ 322.0742; found 322.0644 $[M+H]^+$.

4.2.11. 10-Bromo-5,7,8,13-tetrahydro-6H-azepino[3,4-b:5,6-b']diindol-6-one **14**

Starting from **5**, compound **14** was obtained as pale brown solid using a similar procedure as **10**. Yield 42%; MP: 124–127 °C. IR (neat): ν_{max} 3267, 2926, 2839, 1631, 1486, 1450, 1333, 1014, 744, 445, 407 cm^{-1}; ^1H NMR (500 MHz, $CDCl_3$ + DMSO) δ 11.72 (s, 1H), 11.42 (s, 1H), 8.22 (d, J = 8.0 Hz, 1H), 7.79 (s, 3H), 7.71 (d, J = 1.4 Hz, 1H), 7.61 (d, J = 8.1 Hz, 1H), 7.46 (d, J = 8.6 Hz, 1H), 7.39–7.32 (m, 1H), 7.28–7.21 (m, 1H), 7.19 (dd, J = 8.6, 1.7 Hz, 1H), 4.33 (d, J = 4.6 Hz, 2H). ^{13}C NMR (125 MHz, $CDCl_3$ + DMSO) δ 169.6, 141.6, 140.9,

139.2, 134.8, 132.3, 129.7, 128.3, 128.3, 126.5, 125.4, 124.6, 118.3, 117.7, 117.3, 115.4, 113.6, 40.5; HRMS (ESI): *m/z* calcd for $C_{18}H_{12}BrN_3O$ 366.0237; found 366.0242 [M + H] + .

4.2.12. 10,12-Dimethyl-5,7,8,13-tetrahydro-6H-azepino[3,4-b:5,6-b'] diindol-6-one **15**

Starting from **5**, compound **15** was obtained as greenish yellow solid using a similar procedure as **10**. Yield 75%; MP: 130–133 °C. IR (neat): ν_{max} 3438, 3259, 3156, 2913, 1737, 1480, 1442, 1308, 1172, 840, 740, 577, 565, 513. 442 cm^{-1}; ^1H NMR (500 MHz, $CDCl_3$ + DMSO) δ 11.11 (s, 1H), 10.19 (s, 1H), 8.10 (d, J = 7.9 Hz, 1H), 7.55–7.38 (m, 1H), 7.25 (t, J = 7.7 Hz, 1H), 7.21–7.14 (m, 2H), 6.72 (s, 1H), 4.26 (d, J = 5.2 Hz, 2H), 2.81 (s, 3H), 2.34 (s, 3H). ^{13}C NMR (125 MHz, $CDCl_3$ + DMSO) δ 170.0, 141.6, 140.1, 138.0, 134.0, 133.8, 130.7, 129.7, 128.8, 128.5, 127.1, 125.9, 125.1, 119.5, 117.4, 116.5, 114.8, 40.9, 26.3, 21.9; HRMS (ESI): *m/z* calcd for $C_{20}H_{17}N_3O$ 316.1444; found 316.1454 $[M+H]^+$.

4.2.13. 5-Benzyl-5,7,8,13-tetrahydro-6H-azepino[3,4-b:5,6-b']diindol-6-one **16**

A mixture of *N*-alkylated indoloazepinone **7a** (0.5 mmol) and arylhydrazine hydrochloride **6** (1.5 equiv) was refluxed in glacial acetic acid (2 mL) and ethanol (2 mL). After stirring at 70 °C for 1 h, the reaction mixture was cooled to rt. Concentrated HCl (0.1–0.5 mL) was added and stirring is continued at 70 °C for 7 h. Reaction was monitored by TLC. After cooling to rt, the reaction mixture was poured into a 5% sodium acetate solution (15 mL). The mixture was extracted with EtOAc and concentrated in vacuo. The residue was purified by silica gel column chromatography, eluted with ethyl acetate:hexane (15:85) to afford the titled product **16** as orange solid. Yield 51%; MP: 268–270 °C. IR (neat): ν_{max} 3188, 3029, 1738, 1633, 1451, 1326, 735, 694, 509, 470, 407 cm^{-1}; ^1H NMR (500 MHz, DMSO) δ 11.65 (s, 1H), 8.41 (s, 1H), 8.22 (d, J = 8.1 Hz, 1H), 7.63 (t, J = 7.5 Hz, 2H), 7.53 (d, J = 7.9 Hz, 1H), 7.40 (d, J = 7.2 Hz, 1H), 7.31–7.28 (m, 4H), 7.24–7.21 (m, 1H), 7.18 (d, J = 7.3 Hz, 2H), 7.17–7.14 (m, 1H), 7.10 (t, J = 7.4 Hz, 1H), 5.93 (s, 2H), 4.17 (d, J = 5.9 Hz, 2H). ^{13}C NMR (125 MHz, DMSO) δ 163.8, 139.0, 138.5, 137.6, 132.5, 130.8, 129.0, 127.6, 127.1, 125.6, 125.6, 123.1, 122.1, 121.7, 121.3, 119.8, 118.1, 112.4, 112.3, 112.3, 111.8, 47.8, 35.2; HRMS (ESI): *m/z* calcd for $C_{25}H_{20}N_3O$ 378.1601; found 378.1634 $[M+H]^+$.

4.2.14. 5-Benzyl-10-methyl-5,7,8,13-tetrahydro-6H-azepinoq[3,4-b:5,6-b']diindol-6-one **17**

Starting from **7a**, compound **17** was obtained as mustard yellow solid using a similar procedure as **16**. Yield 60%; MP: 193–194 °C. IR (neat): ν_{max} 3278, 3028, 2914, 1645, 1452, 1331, 1306, 1195, 1029, 800, 744, 700, 580, 450 cm^{-1}; ^1H NMR (500 MHz, DMSO) δ 8.74 (s, 1H), 8.05 (d, J = 7.9 Hz, 1H), 7.40 (s, 1H), 7.38 (s, 2H), 7.35–7.30 (m, 2H), 7.25 (s, 1H), 7.23 (s, 1H), 7.22–7.20 (m, 1H), 7.12 (d, J = 6.9 Hz, 2H), 7.05 (d, J = 8.2 Hz, 1H), 6.38 (s, 1H), 5.89 (s, 2H), 4.22 (d, J = 5.9 Hz, 2H), 2.48 (s, 3H). ^{13}C NMR (125 MHz, DMSO) δ 161.8, 136.7, 136.4, 133.9, 130.4, 128.4, 126.7, 126.2, 125.3, 124.9, 123.6, 123.3, 121.1, 121.0, 120.1, 119.0, 115.5, 110.6, 109.8, 109.6, 109.4, 45.7, 33.1, 19.6; HRMS (ESI): *m/z* calcd for $C_{26}H_{21}N_3O$ 392.1757; found 392.1764 $[M+H]^+$.

4.2.15. 5-Benzyl-10-fluoro-5,7,8,13-tetrahydro-6H-azepino[3,4-b:5,6-b'] diindol-6-one **18**

Starting from **7a**, compound **18** was obtained as pale yellow solid using a similar procedure as **16**. Yield 48%; MP: 136–139 °C. IR (neat): ν_{max} 3277, 3030, 1740, 1643, 1628, 1451, 1331, 1304, 1164, 930, 799, 742, 700, 529, 470, 436 cm^{-1}; ^1H NMR (500 MHz, $CDCl_3$) δ 8.94 (s, 1H), 8.03 (d, J = 8.0 Hz, 1H), 7.42 (dd, J = 8.7, 4.3 Hz, 1H), 7.37–7.33 (m, 2H), 7.25 (s, 1H), 7.21 (dd, J = 10.7, 3.2 Hz, 3H), 7.10 (d, J = 6.7 Hz, 3H), 6.97 (dt, J = 9.0, 2.2 Hz, 1H), 6.36 (t, J = 5.0 Hz, 1H), 5.88 (s, 2H), 4.18 (d, J = 6.0 Hz, 2H). ^{13}C NMR (125 MHz, $CDCl_3$) δ 164.2, 158.4 (d, J = 235.81 Hz), 139.0, 138.0, 134.6, 133.5, 129.4, 128.6, 127.3, 126.6, 125.8, 122.9, 121.6, 120.8, 112.8, 112.2 (d, J = 9.54 Hz), 111.9 (d, J = 4.38 Hz), 111.5, 110.5, 110.3, 102.9 (d, J = 24.04 Hz), 48.5, 36.0; HRMS (ESI): *m/z* calcd for $C_{25}H_{18}FN_3O$ 396.1507; found $[M+H]$ + 396.1518.

4.2.16. 5-Benzyl-10-chloro-5,7,8,13-tetrahydro-6H-azepino[3,4-b:5,6-b'] diindol-6-one **19**

Starting from **7a**, compound **19** was obtained as pale yellow solid using a similar procedure as **16**. Yield 44%; MP: 115–118 °C. IR (neat): ν_{max} 3339, 2944, 2832, 1637, 1583, 1479, 1449, 1332, 1025, 790, 407 cm^{-1}; ^1H NMR (500 MHz, $CDCl_3$) δ 8.83 (s, 1H), 8.04 (d, J = 7.9 Hz, 1H), 7.56 (d, J = 1.7 Hz, 1H), 7.43 (d, J = 7.8 Hz, 1H), 7.40 (d, J = 4.3 Hz, 1H), 7.38 (d, J = 8.1 Hz, 1H), 7.30 (d, J = 7.0 Hz, 1H), 7.28 (s, 1H), 7.25 (s, 1H), 7.22 (d, J = 7.1 Hz, 1H), 7.18 (dd, J = 8.5, 1.8 Hz, 1H), 7.13 (d, J = 7.0 Hz, 2H), 6.38 (s, 1H), 5.91 (s, 2H), 4.23 (d, J = 6.1 Hz, 2H). ^{13}C NMR (125 MHz, DMSO) δ 163.7, 138.8, 138.5, 136.0, 134.1, 131.2, 129.0, 127.1, 127.0, 126.7, 125.7, 123.0, 122.0, 121.5, 117.7, 117.5, 113.7, 112.0, 111.9, 47.8, 35.1; HRMS (ESI): *m/z* calcd for $C_{25}H_{18}ClN_3O$ 434.1036; found 434.1042 $[M + Na]^+$.

4.2.17. 5-Benzyl-10-bromo-5,7,8,13-tetrahydro-6H-azepino[3,4-b:5,6-b'] diindol-6-one **20**

Starting from **7a**, compound **20** was obtained as cream solid using a similar procedure as **16.** Yield 47%; MP: 212–215 °C. IR (neat): ν_{max} 3452, 3162, 3025, 2919, 1639, 1520, 1449, 1329, 1296, 1199, 1031, 893, 793, 739, 726, 479, 434, 407 cm^{-1}; ^1H NMR (500 MHz, $CDCl_3$) δ 11.71 (s, 1H), 8.65 (d, J = 6.6 Hz, 1H), 8.13 (s, 1H), 7.96 (d, J = 9.9 Hz, 26H), 7.88–7.82 (m, 2H), 7.85 (s, 1H), 7.67 (d, J = 4.2 Hz, 2H), 7.64 (d, J = 6.6 Hz, 2H), 7.58 (d, J = 2.4 Hz, 2H), 6.35 (s, 2H), 4.67– 4.52 (m, 2H). ^{13}C NMR (125 MHz, DMSO) δ 163.7, 138.8, 138.5, 136.2, 134.0, 131.2, 129.0, 127.6, 127.4 127.1, 125.7, 124.0, 123.0, 122.0, 121.5, 120.5, 114.2, 112.5, 111.8, 111.7, 47.9, 35.1; HRMS (ESI): *m/z* calcd for $C_{25}H_{18}BrN_3O$ 494.0270; found 494.0276 $[M + K]^+$.

4.2.18. 5-Benzyl-10,12-dimethyl-5,7,8,13-tetrahydro-6H-azepino[3,4-b:5,6-b']diindol-6-one **21**

Starting from **7a**, compound **21** was obtained as buff yellow solid using a similar procedure as **16.** Yield 81%; MP: 220–223 °C. IR (neat): ν_{max} 3229, 3161, 3002, 2912, 1634, 1474, 1441, 1322, 1203, 934, 843, 791, 726, 693, 590, 486, 421 $cm^{-}1$; ^1H NMR (500 MHz, $CDCl_3$) δ 8.42 (s, 1H), 8.07 (d, J = 7.7 Hz, 1H), 7.45 (d, J = 8.3 Hz, 1H), 7.42–7.36 (m, 2H), 7.33–7.28 (m, 2H), 7.22 (d, J = 7.3 Hz, 1H), 7.15 (d, J = 7.3 Hz, 3H), 6.90 (s, 1H), 6.21 (s, 1H), 5.93 (s, 2H), 4.26 (d, J = 6.0 Hz, 2H), 2.58 (s, 3H), 2.46 (s, 3H). ^{13}C NMR (125 MHz, $CDCl_3$) δ 164.2, 139.0, 138.1, 134.9, 132.7, 130.1, 128.6, 127.3, 126.7, 125.7, 125.3, 124.7, 123.2, 123.2, 121.5, 120.8, 120.3, 115.3, 112.2, 111.5, 108.8, 48.5, 36.2, 21.5, 16.8; HRMS (ESI): *m/z* calcd for $C_{27}H_{23}N_3O$ 406.1914; found 406.1927 $[M+H]^+$.

4.2.19. 5-(3-Chlorobenzyl)-5,7,8,13-tetrahydro-6H-azepino[3,4-b:5,6-b'] diindol-6-one **22**

Starting from **7b**, compound **22** was obtained as pale brown solid using a similar procedure as **16.** Yield 53%, pale brown solid; MP: 216–219 °C. IR (neat): ν_{max} 3174, 3008, 1626, 1599, 1474, 1439, 1328, 1207, 934, 779, 738, 679, 565, 463 cm^{-1}; ^1H NMR (500 MHz, $CDCl_3$) δ 8.74 (s, 1H), 8.08 (d, J = 8.0 Hz, 1H), 7.62 (d, J = 7.5 Hz, 1H), 7.51 (d, J = 7.8 Hz, 1H), 7.40 (d, J = 5.7 Hz, 1H), 7.33–7.29 (m, 1H), 7.23 (dd, J = 2.7, 1.3 Hz, 1H), 7.21 (s, 1H), 7.20 (d, J = 1.2 Hz, 1H), 7.20–7.18 (m, 1H), 7.16 (s, 1H), 7.04–7.01 (m, 1H), 6.32 (t, J = 5.5 Hz, 1H), 5.87 (s, 2H), 4.31 (d, J = 6.1 Hz, 2H). ^{13}C NMR (125 MHz, $CDCl_3$) δ 164.1, 140.2, 138.9, 137.1, 134.6, 132.7, 129.9, 129.2, 127.6, 126.9, 126.0, 125.5, 124.9, 123.2, 122.4, 121.8, 121.0, 120.6, 117.9, 113.1, 112.0, 111.5, 111.3, 48.1, 36.1; HRMS (ESI): *m/z* calcd for $C_{27}H_{23}N_3O$ 412.1211; found 412.1218 $[M+H]^+$.

*4.2.20. 5-(3-Chlorobenzyl)-10-methyl-5,7,8,13-tetrahydro-6H-azepino [3,4-b:5,6-b']diindol-6-one **23***

Starting from **7b**, compound **23** was obtained as mustard yellow solid using a similar procedure as **16**. Yield 66%; MP: 145–147 °C. IR (neat): ν_{max} 3282, 1703, 1622, 1598, 1474, 1445, 1330, 1307, 1198, 741, 680, 438 cm^{-1}; ^1H NMR (500 MHz, $CDCl_3$) δ 8.62 (s, 1H), 8.06 (d, J = 8.0 Hz, 1H), 7.40 (s, 1H), 7.39–7.36 (m, 2H), 7.32–7.28 (m, 2H), 7.19 (dd, J = 4.7, 0.9 Hz, 2H), 7.16 (s, 1H), 7.10–7.05 (m, 1H), 7.05–6.99 (m, 1H), 6.31 (s, 1H), 5.86 (s, 2H), 4.28 (d, J = 6.1 Hz, 2H), 2.49 (s, 3H). ^{13}C NMR (125 MHz, $CDCl_3$) δ 164.3, 140.2, 139.0, 135.5, 134.5, 132.7, 129.9, 129.8, 129.7, 127.5, 126.8, 126.5, 126.0, 125.7, 124.9, 124.0, 123.2, 121.7, 121.0, 117.6, 111.6, 111.2, 111.1, 48.1, 36.1, 21.5; HRMS (ESI): *m/z* calcd for $C_{26}H_{20}ClN_3O$ 426.1368; found 426.1378 $[M+H]^+$.

*4.2.21. 5-(3-Chlorobenzyl)-10-fluoro-5,7,8,13-tetrahydro-6H-azepino [3,4-b:5,6-b']diindol-6-one **24***

Starting from **7b**, compound **24** was obtained as mustard yellow solid using a similar procedure as **16**. Yield 55%; MP: 132–135 °C. IR (neat): ν_{max} 3281, 3069, 2946, 1625, 1598, 1475, 1448, 1331, 1200, 1164, 930, 741, 680, 531, 485, 433 cm^{-1}; ^1H NMR (500 MHz, $CDCl_3$) δ 8.75 (s, 1H), 8.05 (d, J = 8.0 Hz, 1H), 7.43 (d, J = 4.3 Hz, 1H), 7.41 (d, J = 3.9 Hz, 1H), 7.39 (d, J = 0.8 Hz, 1H), 7.33–7.28 (m, 2H), 7.23 (d, J = 2.6 Hz, 1H), 7.20 (d, J = 1.2 Hz, 1H), 7.20–7.19 (m, J = 2.3, 1.2 Hz, 1H), 7.14 (s, 1H), 7.04–6.95 (m, J = 11.5, 7.8, 2.1 Hz, 3H), 6.27 (s, 1H), 5.87 (s, 2H), 4.26 (d, J = 6.2 Hz, 2H). ^{13}C NMR (125 MHz, DMSO) δ 163.7, 157.8 (d, J = 231.99 Hz), 141.5, 138.4, 134.3, 134.3, 133.6, 130.9, 130.9, 127.8, 127.1, 125.8, 123.1, 122.1, 121.6, 113.2 (d, J = 9.75 Hz), 112.5, 112.1, 111.7, 109.7 (d, J = 26.56 Hz), 103.1, 102.9, 47.5, 35.2; HRMS (ESI): *m/z* calcd for $C_{25}H_{17}ClFN_3O$ 468.0681; found 468.0687 $[M + K]^+$.

*4.2.22. 10-Chloro-5-(3-chlorobenzyl)-5,7,8,13-tetrahydro-6H-azepino [3,4-b:5,6-b']diindol-6-one **25***

Starting from **7b**, compound **25** was obtained as brwon solid using a similar procedure as **16**. Yield 47%; MP: 135–138 °C. IR (neat): ν_{max} 3258, 1630, 1598, 1474, 1330, 1296, 1199, 1093, 741, 679, 520, 466 cm^{-1}; ^1H NMR (500 MHz, DMSO) δ 11.84 (s, 1H), 8.44 (s, 1H), 8.21 (d, J = 7.9 Hz, 1H), 7.73 (d, J = 2.1 Hz, 1H), 7.63 (d, J = 8.5 Hz, 1H), 7.52 (d, J = 8.5 Hz, 1H), 7.41 (t, J = 7.6 Hz, 1H), 7.34–7.32 (m, 1H), 7.31 (d, J = 2.3 Hz, 1H), 7.30–7.28 (m, 1H), 7.18–7.08 (m, 2H), 5.91 (s, 2H), 4.18 (d, J = 5.9 Hz, 2H). ^{13}C NMR (125 MHz, DMSO) δ 163.7, 141.5, 138.4, 136.0, 134.1, 133.6, 131.1, 130.9, 127.6, 127.1, 126.7, 125.9, 125.8, 124.6, 123.1, 122.1, 121.7, 121.6, 117.5, 113.7, 112.0, 111.9, 111.7, 47.5, 35.1; HRMS (ESI): *m/z* calcd for $C_{25}H_{17}Cl_2N_3O$ 484.0386; found 484.0394 $[M + K]^+$.

*4.2.23. 10-Bromo-5-(3-chlorobenzyl)-5,7,8,13-tetrahydro-6H-azepino [3,4-b:5,6-b']diindol-6-one **26***

Starting from **7b**, compound **26** was obtained as orange solid using a similar procedure as **16**. Yield 49%; MP: 145–148 °C. IR (neat): ν_{max} 3258, 3065, 1632, 1597, 1475, 1446, 1328, 1296, 1200, 1067, 742, 679, 516 cm^{-1}; ^1H NMR (500 MHz, $CDCl_3$ + DMSO) δ 11.86 (s, 1H), 8.44 (s, 1H), 8.21 (d, J = 7.9 Hz, 1H), 7.88 (s, 1H), 7.63 (d, J = 8.3 Hz, 1H), 7.48 (d, J = 8.5 Hz, 1H), 7.41 (t, J = 7.5 Hz, 1H), 7.37–7.30 (m, 4H), 7.25 (s, 1H), 7.12 (d, J = 7.0 Hz, 1H), 5.91 (s, 2H), 4.19 (d, J = 5.3 Hz, 2H). ^{13}C NMR (125 MHz, DMSO) δ 163.7, 141.5, 138.4, 136.3, 133.9, 133.6, 131.1, 130.9, 127.6, 127.4, 127.1, 125.9, 125.8, 124.1, 123.1, 122.1, 121.7, 120.6, 114.2, 112.6, 112.5, 111.9, 111.8, 111.7, 47.5, 35.1; HRMS (ESI): *m/z* calcd for $C_{25}H_{17}BrClN_3O$ 529.9860; found 529.9879 $[M + K]^+$.

*4.2.24. 5-(3-Chlorobenzyl)-10,12-dimethyl-5,7,8,13-tetrahydro-6H-azepino[3,4-b:5,6-b']diindol-6-one **27***

Starting from **7b**, compound **27** was obtained as yellow solid using a similar procedure as **16**. Yield 66%; MP: 244–246 °C. IR (neat): ν_{max} 3241, 3156, 3013, 2914, 1634, 1598, 1473, 1441, 1372, 1321, 1202, 1065, 935, 844, 778, 737, 590 487, 420 cm^{-1}; ^1H NMR (500 MHz, $CDCl_3$) δ 8.45 (s, 1H), 8.08 (d, J = 7.9 Hz, 1H), 7.46 (s, 1H), 7.43–7.37 (m, 1H), 7.34–7.29 (m, 1H), 7.22 (s, 1H), 7.19 (s, 1H), 7.19 (d, J = 1.4 Hz, 1H), 7.16 (s, 1H), 7.06–7.00 (m, 1H), 6.90 (s, 1H), 6.30–6.13 (m, 1H), 5.87 (s, 2H), 4.28 (d, J = 5.8 Hz, 2H), 2.57 (s, 3H), 2.46 (s, 3H). ^{13}C NMR (125 MHz, $CDCl_3$) δ 164.1, 140.2, 138.9, 135.0, 134.5, 132.6, 130.1, 129.9, 129.0, 127.5, 126.9, 125.9, 125.3, 124.9, 124.8, 123.2, 121.7, 121.0, 120.3, 115.3, 113.4, 112.2, 111.3, 48.0, 36.2, 21.5, 16.7; HRMS (ESI): *m/z* calcd for $C_{27}H_{22}ClN_3O$ 478.1088; found 478.1100 $[M + K]^+$.

*4.2.25. 5,7-Dibenzyl-5,7,8,13-tetrahydro-6H-azepino[3,4-b:5,6-b'] diindol-6-one **28***

A mixture of *N,N*-dialkylated indoloazepinone **8a** (0.5 mmol) and arylhydrazine hydrochloride **9** (1.5 equiv) was refluxed in glacial acetic acid (2 mL) and ethanol (2 mL). After stirring at 70 °C for 1 h, the reaction mixture was cooled to rt. Concentrated HCl (0.1–0.5 mL) was added and stirring is continued at 70 °C for 7 h. Reaction was monitored by TLC. After cooling to rt, the reaction mixture was poured into a 5% sodium acetate solution (15 mL). The mixture was extracted with EtOAc and concentrated in vacuo. The residue was purified by silica gel column chromatography, eluted with ethyl acetate:hexane (10:90) to afford the desired product **28** as mustard yellow solid. Yield 65%; MP: 112–115 °C. IR (neat): ν_{max} 3267, 3029, 1734, 1594, 1482, 1450, 1326, 1190, 735, 695, 511, 407 cm^{-1}; ^1H NMR (500 MHz, $CDCl_3$) δ 9.01 (s, 1H), 8.02 (d, J = 8.0 Hz, 1H), 7.53 (d, J = 8.1 Hz, 1H), 7.37 (t, J = 7.9 Hz, 3H), 7.27 (s, 3H), 7.25 (s, 3H), 7.22 (d, J = 7.2 Hz, 1H), 7.16 (s, 1H), 7.14–7.10 (m, 5H), 5.89 (s, 2H), 4.71 (s, 2H), 4.10 (s, 2H). ^{13}C NMR (125 MHz, $CDCl_3$) δ 162.1, 138.9, 138.3, 137.1, 136.9, 133.2, 131.0, 128.7, 128.6, 127.8, 127.4, 127.4, 126.9, 125.9, 125.4, 122.9, 122.1, 121.3, 120.8, 120.3, 117.7, 112.3, 111.4, 111.3, 111.0, 50.9, 48.4, 41.6; HRMS (ESI): *m/z* calcd for $C_{32}H_{25}N_3O$ 506.1629; found 506.1642 $[M + K]^+$.

*4.2.26. 5,7-Dibenzyl-10-methyl-5,7,8,13-tetrahydro-6H-azepino[3,4-b:5,6-b']diindol-6-one **29***

Starting from **8a**, compound **29** was obtained as light orange solid using a similar procedure as **28**. Yield 69%; MP: 210–213 °C. IR (neat): ν_{max} 3233, 3026, 2886, 1628, 1589, 1475, 1449, 1335, 1200, 789, 740, 726, 583, 504, 484, 407 cm^{-1}; ^1H NMR (500 MHz, $CDCl_3$) δ 8.90 (s, 1H), 8.01 (d, J = 8.0 Hz, 1H), 7.40 (d, J = 8.2 Hz, 1H), 7.37–7.32 (m, 2H), 7.31–7.26 (m, 5H), 7.25–7.22 (m, 2H), 7.13–7.09 (m, 5H), 7.04 (dd, J = 8.3, 1.2 Hz, 1H), 5.88 (s, 2H), 4.72 (s, 2H), 4.08 (s, 2H), 2.45 (s, 3H). ^{13}C NMR (125 MHz, $CDCl_3$) δ 162.2, 138.8, 138.3, 137.1, 135.4, 133.3, 130.8, 130.7, 129.5, 128.7, 128.6, 127.9, 127.3, 126.8, 126.1, 125.3, 123.6, 122.9, 121.2, 120.9, 117.4, 112.7, 112.6, 111.1, 110.9, 50.9, 48.3, 41.7, 21.6; HRMS (ESI): *m/z* calcd for $C_{33}H_{28}N_3O$ 482.2232; found 482.2388 $[M+H]^+$.

*4.2.27. 5,7-Dibenzyl-10-fluoro-5,7,8,13-tetrahydro-6H-azepino[3,4-b:5,6-b']diindol-6-one **30***

Starting from **8a**, compound **30** was obtained as mustard yellow solid using a similar procedure as **28**. Yield 51%; MP: 212–214 °C. IR (neat): ν_{max} 3233, 3026, 2886, 1628, 1589, 1475, 1449, 1335, 1200, 789, 740, 726, 583, 504, 484, 407 cm^{-1}; ^1H NMR (500 MHz, $CDCl_3$) δ 9.12 (s, 1H), 7.99 (d, J = 7.9 Hz, 1H), 7.45–7.35 (m, 4H), 7.27 (s, 5H), 7.10 (s, 5H), 6.98–6.91 (m, 2H), 5.88 (s, 2H), 4.70 (s, 2H), 4.03 (s, 2H). ^{13}C NMR (125 MHz, $CDCl_3$) δ 162.0, 158.3 (d, J = 235.63 Hz), 138.8, 138.1, 136.8, 134.9, 133.4, 131.1, 128.9, 128.7, 128.7, 127.9, 127.5, 127.4, 126.8, 126.6, 125.5, 123.8, 123.6, 122.7, 121.4, 120.8, 112.1. 112.0, 111.9, 111.3 (d, J = 4.81 Hz), 111.0, 110.6, 110.3, 110.0, 102.8 (d, J = 24.67 Hz), 50.9, 48.4, 41.5; HRMS (ESI): *m/z* calcd for $C_{27}H_{22}ClN_3O$ 592.0761; found 592.0773 $[M + K]^+$.

4.2.28. 5,7-Dibenzyl-10-chloro-5,7,8,13-tetrahydro-6H-azepino[3,4-b:5,6-b']diindol-6-one **31**

Starting from **8a**, compound **31** was obtained as pale yellow solid using a similar procedure as **28**. Yield 51%, pale yellow solid; MP: 218–220 °C. IR (neat): ν_{max} 3161, 3028, 2895, 1632, 1594, 1586, 1449, 1334, 1298, 1200, 1058, 899, 789, 738, 725, 699, 527, 434, 407 cm^{-1}; ^1H NMR (500 MHz, DMSO) δ 11.92 (s, 1H), 8.21 (d, J = 8.1 Hz, 1H), 7.75 (s, 1H), 7.73 (d, J = 5.7 Hz, 1H), 7.50 (d, J = 8.5 Hz, 1H), 7.44 (t, J = 7.7 Hz, 1H), 7.36–7.28 (m, J = 11.7, 6.0 Hz, 4H), 7.23 (t, J = 6.1 Hz, 3H), 7.19 (d, J = 8.3 Hz, 2H), 7.13 (t, J = 7.7 Hz, 3H), 5.93 (s, 2H), 4.76 (s, 2H), 4.45–4.18 (m, 2H). ^{13}C NMR (125 MHz, $CDCl_3$) δ 162.0, 138.8, 138.1, 136.7, 135.5, 134.4, 131.3, 130.3, 128.7, 128.7, 128.0, 127.6, 127.4, 126.8, 125.6, 124.7, 122.8, 121.5, 120.8, 120.6, 120.4, 120.3, 113.6, 112.7, 111.1, 110.7, 50.9, 48.4, 41.4; HRMS (ESI): m/z calcd for $C_{32}H_{25}ClN_3O$ 502.1686; found 502.1689 $[M+H]^+$.

4.2.29. 5,7-Dibenzyl-10,12-dimethyl-5,7,8,13-tetrahydro-6H-azepino[3,4-b:5,6-b']diindol-6-one **32**

Starting from **8a**, compound **32** was obtained as mustard yellow solid using a similar procedure as **28**. Yield 64%; MP: 130–133 °C. IR (neat): ν_{max} 3279, 3029, 1746, 1634, 1603, 1452, 1331, 1192, 1030, 799, 740, 699, 442, 407 cm^{-1}; ^1H NMR (500 MHz, DMSO) δ 11.35 (s, 1H), 8.21 (d, J = 8.0 Hz, 1H), 7.72 (d, J = 8.5 Hz, 1H), 7.43–7.38 (m, 1H), 7.32–7.27 (m, 4H), 7.25 (d, J = 6.1 Hz, 1H), 7.24–7.22 (m, 2H), 7.21 (s, 1H), 7.17 (dd, J = 7.3, 1.8 Hz, 2H), 7.14–7.10 (m, 2H), 6.77 (s, 1H), 5.91 (s, 2H), 4.73 (s, 2H), 4.26 (s, 2H), 2.55 (s, 3H), 2.36 (s, 3H). ^{13}C NMR (125 MHz, DMSO) δ 161.9, 138.9, 138.6, 138.1, 135.6, 133.0, 131.1, 129.0, 128.8, 128.6, 128.0, 127.6, 127.4, 127.1, 126.1, 125.6, 124.4, 123.1, 122.9, 121.2, 121.0, 115.5, 112.7, 111.7, 111.4, 51.1, 47.8, 42.5, 21.7, 17.6; HRMS (ESI): m/z calcd for $C_{34}H_{29}N_3O$ 496.2389; found 496.2392 $[M+H]^+$.

4.2.30. 5,7-Bis(3-chlorobenzyl)-10-methyl-5,7,8,13-tetrahydro-6H-azepino[3,4-b:5,6-b']diindol-6-one **33**

Starting from **8b**, compound **33** was obtained as light brown solid using a similar procedure as **28**. Yield 58%; MP: 181–183 °C. IR (neat): ν_{max} 3244, 2924, 2854, 1585, 1472, 1454, 1333, 1201, 1123, 794, 772, 744, 690, 681, 434 cm^{-1}; ^1H NMR (500 MHz, $CDCl_3$) δ 8.64 (s, 1H), 8.04 (d, J = 8.0 Hz, 1H), 7.47–7.43 (m, 1H), 7.43–7.40 (m, 1H), 7.39 (d, J = 4.5 Hz, 1H), 7.37 (s, 1H), 7.32–7.28 (m, 1H), 7.23 (d, J = 1.7 Hz, 1H), 7.22 (s, 1H), 7.21–7.20 (m, 1H), 7.19–7.17 (m, 1H), 7.16–7.12 (m, 1H), 7.11 (s, 1H), 7.06 (d, J = 1.0 Hz, 1H), 7.05–7.02 (m, 1H), 7.01 (s, 1H), 5.87 (s, 2H), 4.76 (s, 2H), 4.21 (s, 2H), 2.46 (s, 3H); ^{13}C NMR (125 MHz, $CDCl_3$) δ 162.0, 140.3, 139.3, 138.8, 138.8, 135.4, 134.6, 134.1, 133.1, 130.5, 130.0, 129.9, 129.8, 128.1, 127.6, 127.6, 126.9, 126.0, 125.9, 125.7, 125.0, 123.9, 123.1, 123.0, 121.6, 120.9, 117.4, 113.6, 112.7, 110.0, 110.0, 110.9, 50.7, 48.0, 41.9, 21.5; HRMS (ESI): m/z calcd for $C_{32}H_{22}Cl_3N_3O$ 592.0761; found 592.0773 $[M+H]^+$.

4.2.31. 5,7-Bis(3-chlorobenzyl)-10-fluoro-5,7,8,13-tetrahydro-6H-azepino [3,4-b:5,6-b']diindol-6-one **34**

Starting from **8b**, compound **34** was obtained as brown solid using a similar procedure as **28**. Yield 50%; MP: 210–213 °C. IR (neat): ν_{max} 3325, 2943, 2832, 1598, 1474, 1452, 1335, 1201, 1079, 1025, 742, 681, 433, 410 cm^{-1}; ^1H NMR (500 MHz, $CDCl_3$) δ 8.76 (s, 1H), 8.03 (d, J = 8.0 Hz, 1H), 7.47–7.44 (m, 1H), 7.44–7.41 (m, 2H), 7.24 (s, 1H), 7.22 (s, 1H), 7.21 (d, J = 4.3 Hz, 2H), 7.19 (s, 1H), 7.17 (s, 1H), 7.05 (s, 1H), 7.03 (d, J = 7.6 Hz, 1H), 6.99–6.97 (m, 1H), 6.97–6.93 (m, 2H), 5.87 (s, 2H), 4.76 (s, 2H), 4.19 (s, 2H); ^{13}C NMR (125 MHz, $CDCl_3$) δ 165.6, 161.4 (d, J = 345.60 Hz), 140.1, 139.0, 138.7, 137.0, 134.7, 133.0, 130.3, 130.0, 130.0, 128.0, 127.8, 127.7, 126.9, 126.0, 125.0, 121.8, 120.7, 120.4, 120.2 (d, J = 2.19 Hz), 111.1, 110.51 (d, J = 24.21 Hz), 110.4, 50.7, 48.0, 41.9; HRMS (ESI): m/z calcd for $C_{32}H_{22}Cl_3N_3O$ 592.0761; found 592.0773 $[M+H]^+$.

4.3. Biological assay methods

4.3.1. Cell culture

Cells were obtained from National Centre for Cell Sciences (NCCS), Pune, India and stocks were maintained in the laboratory. Prostate cancer cells (DU143), Liver carcinoma cells (HEPG2), Colon carcinoma cells (RKO) and Lung cancer cells (A549) and human embryonic kidney cells (HEK) were grown in tissue culture flasks in DMEM (Dulbecco Modified Eagle Medium), Sigma or RPMI (Roswell Park Memorial Institute medium) supplemented with 10% fetal bovine serum with 1X stabilized antibiotic–antimycotic solution (Sigma) in a CO_2 incubator at 37 °C with 5% CO_2 and 90% relative humidity.

4.3.2. Evaluation of cytotoxicity with MTT assay

The cytotoxicity of these azepino diindolone derivatives were determined using MTT assay. Cell lines (DU143, HEPG2, RKO, A549 AND HEK-293) were used in this assay. 1X104 cells/well were seeded in 200 μL Dulbecco's modified Eagle's medium (DMEM) supplemented with 10% FBS in each well of 96-well microculture plates and incubated for 24 h at 37 °C in a CO_2 incubator. All the derivatives diluted to the desired concentrations (500 *n*M, 1 μM, 5 μM, 10 μM, 25 μM, 50 μM, 75 μM, 100 μM and 150 μM) in culture medium, were added to the wells with respective vehicle as control. Doxorubicin treated cells, in the same concentration range were used as standards. After 48 h of incubation period, 10 μL MTT (3-(4,5-dimethylthiazol-2-yl)-2,5-diphenyltetrazoliumbromide) (5 mg/mL) was added to each well and the plates were incubated for 4 h. The supernatant was then carefully removed from each well plate and the formed formazon crystals were dissolved in 100 μL of DMSO and the absorbance at 570 nm wavelength was recorded using an ELx800 microplate reader (BioTek, USA). Assay was repeated thrice and mean values were considered.

4.4. Topoisomerase inhibition and DNA binding studies

Topoisomerase assay was performed using the assay kit that is provided by TopoGEN Inc. The assay kit contains human topoisomerase I and IIα enzymes (quantity provided in units), substrate DNA, buffer, proteinase K, SDS and a positive control drug etoposide. Etoposide and camptothecin are provided as lyophilized powders which we need to be reconstituted using DMSO as solvent to form a final concentration of 10 mM. The enzymes need to be preserved at −80 °C.

4.4.1. Decatenation assay

Kinetoplastid DNA (kDNA) (100 ng), buffer (freshly prepared by mixing component A & B), investigational compounds (100 μM) or etoposide (100 μM), and human topoisomerase IIα was added in reaction mixture. Double distilled water was added to make the volume upto 20 μL. The two components of buffer are provided separately that we need to mix immediately before the reaction and thus makes final buffer concentration 5X. Buffer A contained 0.5 M Trish-HCl (pH 8), 1.5 M sodium chloride, 5 mM dithiothreitol, 300 μg/mL bovine serum albumin and buffer B contains 20 mM ATP in water. The reaction mixture was incubated for 30 min at 37 °C. After reaction was complete we stopped the reaction by adding proteinase K (500 μM/mL) and SDS (10%). Incubation for 37 °C for 30 min will complete the digestion. The samples was mixed with 10X loading dye. Resolution of the DNA component was done on 0.8% agarose gel containing 0.5 μg/mL ethidium bromide. Tris-acetate-EDTA buffer (pH 7.4) was employed for the resolution. Visualization and quantification will be performed on Gel DocTM EZ imager (BIO-RAD) and image Lab (BIO-RAD) respectively.

4.4.2. Topoisomerase IIα-Mediated DNA relaxation assay

Supercoiled plasmid DNA (pRYG) was used as substrate. In reaction mixture 200 ng of substrate supercoiled plasmid DNA (pRYG), 5X freshly prepared buffer (premixing component A & B), followed by investigational compounds (100 μM) or standard drug (100 μM) and

lastly human topoisomerase IIα was added. Volume of reaction mixture was adjusted upto 20 μL by adding double distilled water. The final reaction mixture was incubated at 37 °C for 30 min. After completion we stop the reaction by adding proteinase K (500 μM/mL) and SDS (10%) and incubation at 45 °C for 30 min. Electrophoresis will be carried out without ethidium bromide on 1% agarose gel in TAE buffer. Staining of gel with ethidium bromide (0.5 μg/mL) and destaining with water will be carried out. Visualization and quantification will be performed on Gel DocTM EZ imager (BIO-RAD) and image Lab (BIO-RAD), respectively.

4.4.3. Topoisomerase IIα-Mediated DNA cleavage assay

Topo IIα cleavage assay was performed as per the reported protocol [40]. Reaction mixtures (20 μL each) containing 40 mM Tris, pH 7.5, 100 mM KCl, 10 mM $MgCl_2$, 0.5 mM dithiothreitol, 0.5 mM EDTA, 30 μg/mL bovine serum albumin, 50 ng of ^{32}P-labeled DNA (or 20 μg/mL of unlabeled dimeric pRR322 DNA), 20 ng of calf thymus DNA topoisomerase II (or 70 ng of enzyme if unlabeled pBR322 DNA is used), and compounds were incubated at 37 °C for 30 min. The reactions were terminated by the addition of 2 μL of 5% SDS. Unless indicated, reaction mixtures were treated with 150 μg/mL proteinase K for another h at 37 °C.

4.4.4. Topoisomerase I-mediated relaxation assay

Supercoiled DNA pBR322 was used as a substrate in the topoisomerase I-mediated relaxation assay. In 200 ng DNA pBR322 10X buffer (100 mM Tris-HCl (pH-7.9), 10 mM EDTA, 1.5 M sodium chloride, 1% BSA, 1 mM spermidine, 50% glycerol), 100 μM investigational compounds or camptothecin and topoisomerase I was added. The reaction mixture was then incubated at 37 °C for 30 min. Proteinase K (500 μM/mL) and SDS (10%) was added to stop the reaction and further incubation at 50 °C for 20 min will give the digested products. Final DNA products can be resolved on agarose gel (1%). Digested DNA fragments were photographed and analysed by Gel DocTM EZ imager (BIO-RAD).

4.4.5. DNA intercalation assay

DNA intercalation assay was carried out using negatively supercoiled DNA (pUC19) as a substrate. Each reaction mixture contains 200 ng DNA, 100 μM investigational compounds or 1 μM ethidium bromide and double distilled water to make the reaction volume upto 20 μL. After incubation at 37 °C for 30 min, resolution was performed at 1% agarose gel in TAE buffer without ethidium bromide. After the staining and destaining of the gel, the gel was visualized under Gel DocTM EZ imager (BIO-RAD) to observe the retardation.

4.4.6. Circular dichroism

Stock solution of calf thymus DNA (^{CT}DNA) was prepared by dissolving 6 mg/mL in 10 mM Tris-HCl buffer (pH-7.4) and was stored in 4 °C. It was stirred occasionally for 24 h to get homogeneous mixture. The investigational compounds of various concentrations with compound/DNA ratio 1/10, 1/6, 1/4, 1/3 were incubated at 25 °C for 1 h. CD spectra of the complexes were recorded on JASCO-J-815CD Spectrophotometer. Spectra were measured at far-UV (200–320 nm), with band width of 1 nm, path length 0.1 cm at scanning speed 100 nm/min. Three scans were accumulated and averaged. Spectrum of buffer was subtracted from ^{CT}DNA and ^{CT}DNA-compound complex.

4.4.7. UV-Visible spectroscopy

UV-Visible spectra were recorded in LabIndia spectrophotometer with quartz cuvette of having path length 1 nm. Various concentrations of investigational compounds were incubated with ^{CT}DNA (50 μg/mL) at 25 °C for 1 h.

4.5. Morphological observations

A549 cells were seeded at density of 1 × 105 cells/mL in a 6 well plates and were treated with compound **11** at various concentrations (0, 1, 2.5, 5, 10 μM). After 48 h of treatment, morphological changes in the cells were observed and images were captured under a phase contrast microscope (Nikon, Inc. Japan).

4.5.1. Acridine Orange/Ethidium bromide (AO/EB) staining

A549 cells were plated at a concentration of 1x106 cells/mL were treated with compound **11** at concentration of 0, 1, 2.5, 5, 10 μM. Plates were incubated for 48 h at 37 °C. 10 μL each from 1 mg/mL stock solution of fluorescent dyes containing acridine orange (AO) ethidium bromide (EB) were added into each well in equal volumes (10 μg/mL), respectively. Cells were visualized under fluorescence microscope (Nikon, Inc. Japan) with excitation (488 nM) and emission (550 nM) at 200X magnification.

4.5.2. DAPI nucleic acid staining

Nuclear morphological changes were observed by DAPI staining. After treatment with compound **11** (1, 2.5, 5 and 10 μM) for 48 h, A549 cells were washed with PBS and permeabilized with 0.1% Tween 20 for 10 min followed by staining with DAPI. Control and treated cells were observed with fluorescence microscope with excitation at 359 nM and emission at 461 nM using DAPI filter at 200X magnification.

4.6. Flow cytometric analysis

4.6.1. Effect on mitochondrial membrane potential ($\Delta\psi_m$)

6 well plates were seeded with A549 cells (1 × 106 cells/mL) and allowed to adhere for overnight. The cells were incubated with 1.25, 2.5 and 5 μM concentrations of the compound **11** for 48 h. Cells were collected and washed with PBS followed by re-suspension in solution JC-1 (2.5 μg/mL) and incubated for 45 min in incubator at 37 °C. The stained cells were washed twice with PBS and cells were trypsinized, centrifuged and analysed by flow cytometer (BD FACSVerse™, USA).

4.6.2. Cell cycle analysis

Based on the MTT assay, it was clear that compounds **11** exhibited cytotoxicity at 4.2 μM concentration in A549 cells. Flow cytometry analysis (FACS) was performed to evaluate the distribution of the cells under different cell cycle phases. A549 cancer cells were incubated with 1, 2.5, 5 and 10 μM concentrations of the investigated compound **11** for 48 h. Untreated (control) and treated cells were harvested, washed with PBS, fixed in ice-cold 70% ethanol and stained with propidium iodide (PI) (Sigma Aldrich). Cell cycle was performed by flow cytometry (BD FACSVerse™, USA).

4.6.3. Annexin V-FITC/PI assay

A549 cells (1x106 cells/mL) were seeded in six-well plates and allowed to grow overnight. The medium was then replaced with complete medium containing compound **11** at 1, 2.5, 5 and 10 μM concentrations. After 48 h of treatment, cells from the supernatant and adherent monolayer cells were harvested by trypsinization, washed with PBS at 3000 rpm. Then the cells were processed with Annexin V-assay kit (FITC Annexin V Apoptosis Detection Kit, BD PharmingenTM) according to the instructions given by the manufacturer. Further, flow cytometric analysis was performed using a flow cytometer (BD FACSVerse™, USA).

4.7. Molecular docking

Molecular docking studies were performed by using Maestro, version 11.1 of Schrödinger suite 2017-1 [41]. The protein structure of human DNA topoisomerase I (70 kda) in complex with the poison topotecan along with covalent complex with a 22 base pair DNA duplex

(PDB code: 1K4T, resolution 2.1 Å) and the three-dimensional crystal structure of the A-tract DNA dodecamer d(CGCAAATTTGCG) complexed with minor-groove-binding drug Hoechst 33,258 (PDB code: 264D, resolution 2.44 Å) and was obtained from the RCSB PDB. It was prepared using the Protein Preparation Wizard, wherein the protein was hydrogenated and those protons which are necessary to define the correct ionization and tautomerization of protein were also included at pH 7.0. The missing or incomplete residues were repaired by employing the Prime module. OPLS-2005 force field was used to attenuate steric clashes that may exist in the structures under study. The energy minimization was done until the energy was found to converge or the Root Mean Square Deviation (RMSD) reached a maximum cut off of 0.30 Å. Water molecules beyond 5 Å from hetero groups were deleted.

Molecular docking was done keeping the grid box of size 12 Å from the centroid to ensure complete coverage of the active site. To start with, the active site was defined by using the co-crystals of the respective proteins, followed by the validation of docking protocol which was achieved by re-docking the bound-ligand at the active site of human DNA topoisomerase I and DNA. With the validated docking protocol, the investigated compound is docked at the active sites of human DNA topoisomerase I and DNA and the results were compared with their respective co-crystallized ligands.

Acknowledgments

Authors are thankful to NIPER Hyderabad for facilities. MK, PG, DKS and PNM thank Department of Pharmaceuticals (DoP), Ministry of Chemicals & Fertilizers, Govt. of India, New Delhi, for the award of Research fellowships.

Appendix A. Supplementary material

Supplementary data to this article can be found online at https://doi.org/10.1016/j.bioorg.2020.103629.

References

[1] R. Martinez, L. Chacon-Garcia, The search of DNA-intercalators as antitumoral drugs: What it worked and what did not work, Curr. Med. Chem. 12 (2005) 127–151.
[2] Y. Pommier, DNA topoisomerase I inhibitors: chemistry, biology, and interfacial inhibition, Chem. Rev. 109 (2009) 2894–2902.
[3] A.T. Baviskar, C. Madaan, R. Preet, P. Mohapatra, V. Jain, A. Agarwal, S.K. Guchhait, C.N. Kundu, U.C. Banerjee, P.V. Bharatam, *N*-fused imidazoles as novel anticancer agents that inhibit catalytic activity of topoisomerase IIα and induce apoptosis in G1/S phase, J. Med. Chem. 54 (2011) 5013–5030.
[4] C.A. Austin, K.L. Marsh, Eukaryotic DNA topoisomerase IIβ, BioEssays 20 (1998) 215–226.
[5] J.C. Wang, Cellular roles of DNA topoisomerases: a molecular perspective, Nat. Rev. Mol. Cell Biol. 3 (2002) 430–440.
[6] M.M. Aleksić, V. Kapetanović, An overview of the optical and electrochemical methods for detection of DNA - Drug interactions, Acta Chim. Slov. 61 (2014) 555–573.
[7] C. Zimmer, U. Wähnert, Nonintercalating DNA-binding ligands: Specificity of the interaction and their use as tools in biophysical, biochemical and biological investigations of the genetic material, Prog. Biophys. Mol. Biol. 47 (1986) 31–112.
[8] J. Akhtar, A.A. Khan, Z. Ali, R. Haider, M. Shahar Yar, Structure-activity relationship (SAR) study and design strategies of nitrogen-containing heterocyclic moieties for their anticancer activities, Eur. J. Med. Chem. 125 (2017) 143–189.
[9] (a) J. Yan, J. Hu, B. An, L. Huang, X. Li, Design, synthesis, and biological evaluation of cyclic-indole derivatives as anti-tumor agents via the inhibition of tubulin polymerization, Eur. J. Med. Chem. 125 (2017) 663–675;
(b) D. Kumar, V. Pooladanda, P. Singh, M. Kadagathur, Discovery of certain benzyl/phenethyl thiazolidinone-indole hybrids as potential anti-proliferative agents: synthesis, molecular modeling and tubulin polymerization inhibition study, Bioorg. Chem. 92 (2019) 103188.
[10] (a) T. Fukuda, Y. Nanjo, M. Fujimoto, K. Yoshida, Y. Natsui, F. Ishibashi, F. Okazaki, H. To, M. Iwao, Lamellarin-inspired potent topoisomerase I inhibitors with the unprecedented benzo[g][1]benzopyrano[4,3-b]indol-6(13H)-one scaffold, Bioorg. Med. Chem. 27 (2019) 265–277;
(b) J. Kovvuri, B. Nagaraju, V.L. Nayak, R. Akunuri, M.P.N. Rao, A. Ajitha, N. Nagesh, A. Kamal, Design, synthesis and biological evaluation of new β-carboline-bisindole compounds as DNA binding, photocleavage agents and topoisomerase I inhibitors, Eur. J. Med. Chem. 143 (2018) 1563–1577.
[11] E. Rajanarendar, M.N. Reddy, K.R. Murthy, P. Surendar, R.N. Reddy, Y.N. Reddy, Synthesis and *in vitro* and *in vivo* anticancer activity of novel phenylmethylene bis-isoxazolo [4,5-*b*] azepines, Bioorg. Med. Chem. Lett. 22 (2012) 149–153.
[12] T.A. Larsen, D.S. Goodsell, D. Cascio, K. Grzeskowiak, R.E. Dickerson, The structure of DAPI bound to DNA, J. Biomol. Struct. Dyn. 7 (1989) 477–491.
[13] P.G. Baraldi, A. Bovero, F. Fruttarolo, D. Preti, M.A. Tabrizi, M.G. Pavani, R. Romagnoli, DNA minor groove binders as potential antitumor and antimicrobial agents, Med. Res. Rev. 24 (2004) 475–528.
[14] G.R. Pettit, J.C. Knight, D.L. Herald, R. Davenport, R.K. Pettit, B.E. Tucker, J.M. Schmidt, Isolation of labradorins 1 and 2 from Pseudomonas syringae pv. coronafaciens, J. Nat. Prod. 65 (2002) 1793–1797.
[15] P. Russo, C. Nastrucci, A. Cesario, From the Sea to Anticancer Therapy, Curr. Med. Chem. 18 (2011) 3551–3562.
[16] (a) F.J. Schmitz, S.P. Gunasekera, V. Lakshmi, L.M.V. Tillekeratne, J. Nat. Prod. 48 (1985) 47–53;
(b) A.W. White, N. Carpenter, J.R.P. Lottin, R.A. McClelland, R.I. Nicholson, Synthesis and evaluation of novel anti-proliferative pyrroloazepinone and indoloazepinone oximes derived from the marine natural product hymenialdisine, Eur. J. Med. Chem. 56 (2012) 246–253.
[17] L. Meijer, A.M.W.H. Thunnissen, A.W. White, M. Garnier, M. Nikolic, L.H. Tsai, J. Walter, K.E. Cleverley, P.C. Salinas, Y.Z. Wu, J. Biernat, E.M. Mandelkow, S.H. Kim, G.R. Pettit, Inhibition of cyclin-dependent kinases, GSK-3β and CK1 by hymenialdisine, a marine sponge constituent, Chem. Biol. 7 (2000) 51–63.
[18] G.M. Sharma, J.S. Buyer, M.W. Pomerantz, Characterization of a yellow compound isolated from the marine sponge Phakellia flabellata, J. Chem. Soc. Chem. Commun. 23 (1980) 435–436.
[19] G. Cimino, S. De Rosa, S. De Stefano, L. Mazzarella, R. Puliti, G. Sodano, Isolation and X-ray crystal structure of a novel bromo-compound from two marine sponges, Tetrahedron Lett. 23 (1982) 767–768.
[20] D.H. Williams, D. John Faulkner, Isomers and tautomers of hymenialdisine and debromohymenialdisine, Nat. Prod. Lett. 9 (1996) 57–64.
[21] T. Nguyen, J. Tepe, Preparation of hymenialdisine, analogues and their evaluation as kinase inhibitors, Curr. Med. Chem. 16 (2009) 3122–3143.
[22] Y. Wan, W. Hur, C.Y. Cho, F.J. YiLiu, O. Adrian, S. Lozach, S. Gray Bach, Synthesis and target identification of hymenialdisine analogs, Chem. Biol. 11 (2004) 247–259.
[23] V. Sharma, J.J. Tepe, Potent inhibition of checkpoint kinase activity by a hymenialdisine-derived indoloazepine, Bioorg. Med. Chem. Lett. 14 (2004) 4319–4321.
[24] D.W. Zaharevitz, R. Gussio, M. Leost, A.M. Senderowicz, T. Lahusen, C. Kunick, L. Meijer, E.A. Sausville, Discovery and initial characterization of the paullones, a novel class of small- molecule inhibitors of cyclin-dependent kinases, Cancer Res. 59 (1999) 2566–2569.
[25] L. Joucla, L. Picot, T. Besson, Synthesis of latonduine derivatives *via* intramolecular Heck reaction, Tetrahedron. 63 (2007) 867–879.
[26] J. Xie, J. Tian, L. Su, M. Huang, X. Zhu, F. Ye, Y. Wan, Pyrrolo[2,3-*c*]azepine derivatives: a new class of potent protein tyrosine phosphatase 1B inhibitors, Bioorg. Med. Chem. Lett. 21 (2011) 4306–4309.
[27] (a) A.K. Singh, V. Raj, S. Saha, Indole-fused azepines and analogues as anticancer lead molecules: privileged findings and future directions, Eur. J. Med. Chem. 142 (2017) 244–265;
(b) L.F. Tietze, H.P. Bell, S. Chandrasekhar, Natural product hybrids as new leads for drug discovery, Angew. Chemie - Int. Ed. 42 (2003) 3996–4028;
(c) B.J. Pleuvry, Pharmacodynamic and pharmacokinetic drug interactions, Anaesth. Intensive Care Med. 6 (2005) 129–133.
[28] (a) B. Meunier, Hybrid molecules with a dual mode of action: Dream or reality? Acc. Chem. Res. 41 (2008) 69–77;
(b) R. Morphy, Z. Rankovic, Designed multiple ligands. an emerging drug discovery paradigm, J. Med. Chem. 48 (2005) 6523–6543;
(c) S. Shaveta, P. Mishra, Singh, hybrid molecules: the privileged scaffolds for various pharmaceuticals, Eur. J. Med. Chem. 124 (2016) 500–536.
[29] V. Sharma, T.A. Lansdell, G. Jin, J.J. Tepe, Inhibition of cytokine production by hymenialdisine derivatives, J. Med. Chem. 3700–3703 (2004).
[30] B. Robinson, The fischer indole synthesis, Chem. Rev. 63 (1963) 373–401.
[31] Y. Pommier, Drugging topoisomerases: Lessons and challenges, ACS Chem. Biol. 8 (2013) 82–95.
[32] (a) G. Priyadarshani, S. Amrutkar, A. Nayak, U.C. Banerjee, C.N. Kundu, S.K. Guchhait, Scaffold-hopping of bioactive flavonoids: Discovery of aryl-pyridopyrimidinones as potent anticancer agents that inhibit catalytic role of topoisomerase IIα, Eur. J. Med. Chem. 122 (2016) 43–54;
(b) G. Priyadarshani, A. Nayak, S.M. Amrutkar, S. Das, S.K. Guchhait, C.N. Kundu, U.C. Banerjee, Scaffold-Hopping of Aurones: 2-Arylideneimidazo[1,2-a]pyridinones as Topoisomerase IIα-Inhibiting Anticancer Agents, ACS Med. Chem. Lett. 7 (2016) 1056–1061;
(c) A.T. Baviskar, S.M. Amrutkar, N. Trivedi, V. Chaudhary, A. Nayak, S.K. Guchhait, U.C. Banerjee, P.V. Bharatam, C.N. Kundu, Switch in site of inhibition: a strategy for structure-based discovery of human topoisomerase IIα catalytic inhibitors, ACS Med. Chem. Lett. 6 (2015) 481–485;
(d) G. Darpan, S.M. Joshi, A.T. Amrutkar, H. Baviskar, S. Kler, U.C. Singh, R. Banerjee Kumar, , Synthesis and biological evaluation of new 2,5-dimethylthiophene/furan based N-acetyl pyrazolines as selective topoisomerase II inhibitors, RSC Adv. 6 (2016) 14880–14892.
[33] (a) A. Kellett, Z. Molphy, C. Slator, V. McKee, N.P. Farrell, Molecular methods for assessment of non-covalent metallodrug-DNA interactions, Chem. Soc. Rev. 48 (2019) 971–988;
(b) D.K. Jangir, S. Charak, R. Mehrotra, S. Kundu, FTIR and circular dichroism spectroscopic study of interaction of 5-fluorouracil with DNA, J. Photochem. Photobiol. B Biol. 105 (2011) 143–148;

(c) W. Zhong, J.S. Yu, Y. Liang, K. Fan, L. Lai, Chlorobenzylidine-calf thymus DNA interaction II: Circular dichroism and nuclear magnetic resonance studies, Spectrochim. Acta Part A Mol. Biomol. Spectrosc. 60 (2004) 2985–2992.

[34] I. Ahmad, M. Ahmad, Dacarbazine as a minor groove binder of DNA: Spectroscopic, biophysical and molecular docking studies, Int. J. Biol. Macromol. 79 (2015) 193–200.

[35] (a) M. Rahban, A. Divsalar, A.A. Saboury, A. Golestani, nanotoxicity and spectroscopy studies of silver nanoparticle: Calf thymus DNA and K562 as targets, J. Phys. Chem. C. 114 (2010) 5798–5803;
(b) R. Tokala, S. Thatikonda, S. Sana, P. Regur, C. Godugu, N. Shankaraiah, Synthesis and in vitro cytotoxicity evaluation of β-carboline-linked 2,4-thiazolidinedione hybrids: potential DNA intercalation and apoptosis-inducing studies, New J. Chem. 42 (2018) 16226–16236.

[36] K. Liu, P. Cheng Liu, R. Liu, X. Wu, Dual AO/EB staining to detect apoptosis in osteosarcoma cells compared with flow cytometry, Med. Sci. Monit. Basic Res. 21 (2015) 15–20.

[37] J.D. Ly, D.R. Grubb, A. Lawen, The mitochondrial membrane potential (Δψm) in apoptosis; an update, Apoptosis 8 (2003) 115–128.

[38] C. Riccardi, I. Nicoletti, Analysis of apoptosis by propidium iodide staining and flow cytometry, Nat. Protoc. 1 (2006) 1458–1461.

[39] M. Eray, M. Mattö, M. Kaartinen, L.C. Andersson, J. Pelkonen, Flow cytometric analysis of apoptotic subpopulations with a combination of Annexin V-FITC, propidium iodide, and SYTO 17, Cytometry. 43 (2001) 134–142.

[40] Y.H. Hsiang, R. Hertzberg, S. Hecht, L.F. Liu, Camptothecin induces protein-linked DNA breaks *via* mammalian DNA topoisomerase I, J. Biol. Chem. 260 (1985) 14873–14878.

[41] Glide, Schrödinger, LLC, New York, NY, 2017.